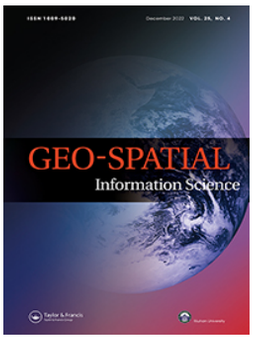

Geo-spatial Information Science

ISSN: (Print) (Online) Journal homepage: https://www.tandfonline.com/loi/tgsi20

Exploiting satellite SAR for archaeological prospection and heritage site protection

Francesca Cigna, Timo Balz, Deodato Tapete, Gino Caspari, Bihong Fu, Michele Abballe & Haonan Jiang

To cite this article: Francesca Cigna, Timo Balz, Deodato Tapete, Gino Caspari, Bihong Fu, Michele Abballe & Haonan Jiang (2023): Exploiting satellite SAR for archaeological prospection and heritage site protection, Geo-spatial Information Science, DOI: 10.1080/10095020.2023.2223603

To link to this article: https://doi.org/10.1080/10095020.2023.2223603

Published online: 25 Jul 2023.

GEO-SPATIAL INFORMATION SCIENCE
https://doi.org/10.1080/10095020.2023.2223603

Taylor & Francis
Taylor & Francis Group

Exploiting satellite SAR for archaeological prospection and heritage site protection

Francesca Cigna[a], Timo Balz[b], Deodato Tapete[c], Gino Caspari[d], Bihong Fu[e], Michele Abballe[a] and Haonan Jiang[b]

[a]National Research Council, Institute of Atmospheric Sciences and Climate (CNR-ISAC), Rome, Italy; [b]State Key Laboratory of Information Engineering in Surveying, Mapping and Remote Sensing (LIESMARS), Wuhan University, Wuhan, China; [c]Italian Space Agency (ASI), Rome, Italy; [d]Department of Archaeology, University of Sydney, Sydney, Australia; [e]Aerospace Information Research Institute, Chinese Academy of Sciences (AIR-CAS), Beijing, China

ABSTRACT

Optical and Synthetic Aperture Radar (SAR) remote sensing has a long history of use and reached a good level of maturity in archaeological and cultural heritage applications, yet further advances are viable through the exploitation of novel sensor data and imaging modes, big data and high-performance computing, advanced and automated analysis methods. This paper showcases the main research avenues in this field, with a focus on archaeological prospection and heritage site protection. Six demonstration use-cases with a wealth of heritage asset types (e.g. excavated and still buried archaeological features, standing monuments, natural reserves, burial mounds, paleo-channels) and respective scientific research objectives are presented: the Ostia-Portus area and the wider Province of Rome (Italy), the city of Wuhan and the Jiuzhaigou National Park (China), and the Siberian "Valley of the Kings" (Russia). Input data encompass both archive and newly tasked medium to very high-resolution imagery acquired over the last decade from satellite (e.g. Copernicus Sentinels and ESA Third Party Missions) and aerial (e.g. Unmanned Aerial Vehicles, UAV) platforms, as well as field-based evidence and ground truth, auxiliary topographic data, Digital Elevation Models (DEM), and monitoring data from geodetic campaigns and networks. The novel results achieved for the use-cases contribute to the discussion on the advantages and limitations of optical and SAR-based archaeological and heritage applications aimed to detect buried and sub-surface archaeological assets across rural and semi-vegetated landscapes, identify threats to cultural heritage assets due to ground instability and urban development in large metropolises, and monitor post-disaster impacts in natural reserves.

ARTICLE HISTORY
Received 27 January 2023
Accepted 6 June 2023

KEYWORDS
Synthetic Aperture Radar (SAR); interferometric SAR (InSAR); multispectral imagery; cultural heritage; crop mark; archaeological prospection; site monitoring; Unmanned Aerial vehicle (UAV) surveying

1. Introduction

The use of remote sensing for archaeological and cultural heritage applications has a long history, enabling to outline the trajectory that this scientific field has followed over the past century (Luo et al. 2019). In this framework, imaging radar, and in particular, Synthetic Aperture Radar (SAR) technologies, have played a key role in advancing the application field of cultural heritage (Chen et al. 2022). As a discipline, imaging radar has reached such a level of maturity that the stage of proof-of-concept has been successfully passed, and several operational workflows have been established to address user-driven real-world applications in the framework of interdisciplinary approaches (Chen et al. 2021).

It is in this context, wherein both the European and the Chinese scientific communities have consolidated shared technical expertise in SAR for cultural heritage, that the present paper aims to showcase the research avenues that are currently investigated to further advance the exploitation of satellite SAR data for purposes of archaeological prospection and heritage site protection. To better frame the novelty of this paper, a brief account of the current state-of-the-art of SAR remote sensing for heritage applications is first provided (Section 1.1), also in relation to optical remote sensing that is used to complement SAR observations and measurements. Specific scientific objectives of the collaborative research context framing the work are then provided (Section 1.2), toward the presentation of data and methods (Section 2), results and discussion (Section 3), and key conclusions (Section 4).

1.1. Optical and radar imaging for heritage applications: state-of-the-art

In the last decades, Earth Observation (EO) technologies and imagery collected by means of space-borne sensors – mainly operating in the visible, InfraRed (IR), and microwave portions of the electromagnetic spectrum – have been increasingly used for cultural heritage applications. These encompass investigations

CONTACT Francesca Cigna f.cigna@isac.cnr.it

aimed at site discovery, documentation, monitoring, condition reporting (Agapiou and Lysandrou 2015; Lasaponara and Masini 2012) and, more recently, damage assessment and disaster risk management (Agapiou, Lysandrou, and Hadjimitsis 2020). In a sort of technological continuity with the much longer tradition relying on the use of aerial photographs, nowadays many archaeologists, heritage scientists, and practitioners are also familiar with satellite images.

The evidence found in the scientific literature clearly shows a user preference for High and Very High Resolution (HR and VHR) optical imagery, dominantly collected in the visible and Near-IR (NIR) channels, less in the short-wave infrared or other bands (e.g. Tapete and Cigna 2019b). These data are accessed from open visualization and/or processing platforms (e.g. Bing Maps, Google Earth Pro, Google Earth Engine; Luo et al. 2018) or via data grants or (albeit, less common) direct purchase from commercial providers. One of the properties most appreciated by end-users is the provision of these data in pre-processed (e.g. orthorectified, pansharpened) or analysis-ready formats (e.g. geocoded raster), directly enabling further handling and analysis, for example, in Geographic Information System (GIS) environments. This trend is common across different application domains, e.g., archaeological prospection of buried features, site detection, digital surveying, and inventorying over wide areas, and damage assessment in crisis scenarios (for instance, due to looting or warfare). The need for a high spatial resolution to document the finest details of a given monument, site, or cultural landscape, and for dedicated surveys to be undertaken during specific field seasons at a relatively low cost, has also stimulated archaeologists and practitioners to use Unmanned Aerial Vehicles (UAVs) or drones. Their role in archaeological surveying of excavations and landscapes, and diagnostics more generally, is growing inexorably (Campana 2017).

At the same time, the above developments and opportunities have contributed to making Medium Resolution (MR) data (e.g. Landsat) progressively less appealing for archaeological applications, especially at the local and site scale. For some strands of the archaeological community (e.g. McGrath et al. 2020), even optical HR data collections such as those provided by Copernicus Sentinel–2 at 10 m resolution cannot provide the necessary ground sampling distance for archaeological purposes like archaeological prospection and crop mark detection. Contrasting evidence is provided by another research strand that, instead, is unveiling the added value of high-temporal revisit constellations (e.g. Sentinel–2) for monitoring and condition assessment of cultural heritage sites during both ordinary and crisis time (Tapete and Cigna 2018), in the context of modern activities that may threaten conservation (Conesa et al. 2022; Rayne et al. 2020), and for regional archaeological surveying (Bini et al. 2018; Orengo et al. 2020; Tapete et al. 2021b). This growing literature proves that Sentinel –2 can be a source of geospatial information to complement other datasets and support studies focused on open-air and standing archaeological heritage. On the contrary, still limited is the published literature on buried remains which mostly refers to linear ancient structures and infrastructure (e.g. Lasaponara, Abate, and Masini 2022; Zanni and De Rosa 2019). Therefore, a topic that needs to be more deeply investigated is the potential of HR multispectral data, either alone or in combination with other VHR optical imagery and/or SAR, for archaeological prospection and crop mark detection.

In this respect, the integration of optical imagery with other sensor data could also build upon the lessons learned on the use of satellite SAR to address studies of archaeological landscapes, archaeological prospection, and condition assessment of cultural heritage, as documented in the substantial body of literature that has been increasingly published since 1985 (Tapete and Cigna 2017b). In addition to the intrinsic capability of operating under any weather conditions, the advantageous properties offered by SAR include: wide-swath to spotlight coverage, kilometer to sub-meter spatial resolution, historical and present-day temporal coverage, longer to shorter wavelength (e.g. L/C/X bands), monthly to daily revisiting time if collecting time series (Tapete and Cigna 2017b). These properties have been even further improved from earlier (e.g. ERS–1/2, ENVISAT, ALOS–1, RADARSAT–1) to current satellite missions (e.g. TerraSAR-X, COSMO-SkyMed First and Second Generation, Sentinel–1 and ALOS–2).

Such wealth of SAR data and increased accessibility to image archives and tasking opportunities have contributed to stimulating significant research development for cultural heritage applications (Chen et al. 2022). In the field of archaeological prospection, Wiseman and El-Baz (2007) and references therein provide an exemplary collection of pioneering studies exploiting the peculiar penetration capability of the radar signal at different wavelengths and demonstrating that better performance is usually obtained at longer wavelengths (e.g. L band) and in drier and fine-grained soils. More recent research has also proved that, under certain surface roughness, soil moisture content, and surface land cover conditions, even imagery collected at shorter wavelengths such as X-band (often provided at HR to VHR, nowadays reaching up to <1 m resolution) can unveil “shadow marks”, “crop marks”, and “soil and damp marks”. This can be achieved, for instance, via speckle filtering techniques applied to single images (Chen et al. 2015),

or detection of anomalies in multi-temporal SAR series collected across seasons (Tapete and Cigna 2019a). Although archaeological prospection research has already been undertaken in both arid and vegetated environments, the capabilities of SAR on the former have been investigated more than on the latter, thus leaving a research avenue that requires further testing.

There is no doubt that the increased spatial resolution offered by new SAR technological advancements was among the enabling factors to attempt successfully novel applications on cultural heritage. The demonstration is provided by results achieved with the submeter resolution TerraSAR-X Staring Spotlight imaging mode, for example, to assess the discernibility of burial mounds (Balz et al. 2016), and spatial and temporally track the damage due to illegal excavations (Tapete, Cigna, and Donoghue 2016).

For monitoring purposes, equally important is the temporal frequency of observation that SAR missions can guarantee, by collecting imagery either according to pre-defined observation scenarios (e.g. Copernicus Sentinel−1) or via tasked acquisitions (e.g. COSMO-SkyMed). The availability of repeated SAR acquisitions, background image collections, and continuous and long time series was exploited to develop tailored change detection approaches enabling the documentation of impacts due to environmental processes and anthropogenic activities (Cigna et al. 2013; Tapete et al. 2013), as well as unexpected incidents that would have been missed, if no regular observations were made (Cigna and Tapete 2018; Tapete and Cigna 2020). Not to forget, that the growing SAR image archives have fueled the testing and improvement of advanced Interferometric SAR (InSAR) chains, to unveil the full potential of SAR for surface deformation analysis and structural health monitoring of archaeological heritage and historical buildings. This has been observed starting from earlier conceptualizations and use-case developments for instance in Rome, Italy (Tapete et al. 2012), up to more advanced approaches applied to cultural heritage in Asia (e.g. Chen et al. 2021, 2022), resulting in a substantial stock of geospatial information produced across and beyond Europe (Tapete and Cigna 2017a). In this respect, other aspects that deserve further investigation to advance SAR data exploitation in this application field include more experimentation on cost-effective processing of big SAR datasets through High-Performance Computing (HPC) and cloud-based infrastructure; development of efficient InSAR time series fusion approaches; and understanding of how InSAR-derived parameters (e.g. surface height) can be used as proxies to document urban development and other land surface processes potentially impacting cultural heritage.

1.2. Dragon−5 SARchaeology project and research aims

Accounting for the state-of-the-art reviewed in Section 1.1, the specific aim of this research paper is to provide a range of SAR-based applications demonstrating improved approaches to exploit these data to map, monitor, and support condition assessment and safeguarding of archaeological, cultural, and natural heritage sites. These activities are carried out in the framework of the project "SARchaeology: exploiting satellite SAR for archaeological prospection and heritage site protection", funded in 2020 as part of the 5th phase of the Dragon cooperation program (namely, Dragon−5; https://dragon5.esa.int/) by the European Space Agency (ESA) and the National Remote Sensing Center of China (NRSCC), under the Ministry of Science and Technology (MOST).

SARchaeology is led by a Sino-European team of scientists from Wuhan University's State Key Laboratory of Information Engineering in Surveying, Mapping and Remote Sensing (LIESMARS) in China, the National Research Council of Italy – Institute of Atmospheric Sciences and Climate (CNR-ISAC), the Italian Space Agency (ASI), the Aerospace Information Research Institute at the Chinese Academy of Sciences (AIR-CAS), and the Archaeology Department at the University of Sydney in Australia. The key scientific goal of the project is to exploit satellite SAR imagery and advanced processing methods for archaeological prospection and heritage site protection. In particular, the project aspires to make step-changes to demonstrate the capabilities of MR to VHR SAR data to detect (semi-)buried and sub-surface objects of archaeological significance and monitor the status and stability of cultural and natural heritage sites and their assets. These goals contribute to the Solid Earth research domain of the Dragon cooperation program and, more in general, are EO applications of paramount importance in the field of land monitoring and Earth system science.

This paper presents the general methodological background (Section 2) and the main scientific results of SARchaeology after 2 years of research at the mid-term stage of the Dragon−5 cooperation, with a focus on the activities that have been kicked off since 2020 and the results achieved for six demonstration use-cases (Sections 3.1-3.6). These encompass study sites in Italy, China, and Russia, and a wealth of heritage asset types, including already excavated and still buried archaeological ruins, standing monuments within urban centers, natural reserves, burial mounds, paleo-channels, and ice patches with organic remains. They thus provide a good representation of geographic areas and heritage assets to demonstrate the analysis methodologies and contribute to the discussion on the advantages and

limitations of SAR-based applications for archaeology, cultural, and natural heritage.

2. Data and methods

Table 1 provides an overview of the specific data types and sources used for each use-case, along with the data analysis and processing approaches implemented to extract information on heritage assets and derive value-added products. Overall, the input data exploited for the demonstration use-cases encompass three main types: archive and/or newly tasked MR, HR, and VHR (i) SAR and (ii) optical imagery acquired by sensors on-board satellite and aerial (including UAV) platforms, plus (iii) other ancillary and monitoring data. The latter include field-based evidence and ground truth (e.g. photographs of asset type and any damage; vegetation/crop type, height, and status), geodetic measurements and time series from permanent Global Navigation Satellite System (GNSS) or Global Positioning System (GPS) stations, benchmarking and leveling monitoring campaigns.

The key sources of satellite SAR and optical imagery are the Copernicus Sentinels fleet (e.g. Sentinel−1 SAR and Sentinel−2 multispectral), ESA Third Party Missions (e.g. TerraSAR-X, COSMO-SkyMed, ALOS−1 and RADARSAT−2 SAR, and WorldView−2, PlanetScope, and SkySat multispectral) and, in future stages of the project, Chinese missions (e.g. Jilin−1 multispectral and CBERS−4 panchromatic). VHR imagery freely available through Google Earth, ESRI, and Bing Maps is also often used as a basemap to visualize and interpret other geospatial data and derived products, along with OpenStreetMap topographic layers, and auxiliary Digital Elevation (DEM), Terrain (DTM) and/or Surface (DSM) Models.

SAR data are analyzed using conventional preprocessing workflows including focusing from raw to single-look complex, radiometric calibration, co-registration, multi-looking (with range and azimuth factors depending on the SAR data source and resolution), and spatial/temporal image filtering. When applicable, change detection based on SAR amplitude and/or interferometric coherence is carried out in the radar geometry (e.g. Cigna et al. 2013; Ruescas et al. 2009). Advanced multi-temporal processing with Persistent Scatterers InSAR (PS-InSAR) (e.g. Crosetto et al. 2016; Ferretti, Prati, and Rocca 2001) or Small BAseline Subset (SBAS) InSAR methods (e.g. Berardino et al. 2002; Lanari et al. 2004) may follow, depending on the specific scientific goals of the use-case (e.g. for stability

Table 1. Summary of the project Areas of Interest (AOIs) and the respective scientific goals of the use-cases, exploited input datasets, and analysis methodologies used.

AOI	Scientific goal	Input datasets	Methodologies
Province of Rome (Italy)	archaeological prospection (see Section 3.1)	SAR: L-band ALOS−1 PALSAR Fine Beam dual-pol. (HH, HV), C-band Sentinel−1 IW and RADARSAT−2 Fine Beam dual-pol. (VV, VH), and X-band COSMO-SkyMed SpotLight single-pol. (VV) imagery Optical: Google Earth, ESRI and Bing VHR base maps, Sentinel−2, PlanetScope, SkySat, Pléiades and WorldView−2 multispectral imagery, and historical aerial photographs Other: field evidence on vegetation status, ploughing/harvesting activity, crop/soil marks visibility	feature identification; spectral analysis and indices (e.g. NDVI); crop marks detection; multi-temporal analysis
	ground stability monitoring (see Section 3.2)	SAR: C-band Sentinel−1 IW dual-pol. (VV, VH) imagery Optical: Google Earth VHR imagery and ESRI base maps Other: site photographs with evidence of structural damage	parallelized SBAS InSAR; data analytics
Wuhan (China)	urban development monitoring (see Section 3.3)	SAR: X-band COSMO-SkyMed StripMap single-pol. (HH) imagery Optical: Google Earth VHR and declassified Keyhole imagery Other: field evidence	PS-InSAR and dynamic tPS height estimation
	ground stability monitoring (see Section 3.4)	SAR: X-band TerraSAR-X and COSMO-SkyMed StripMap single pol. (HH), and C-band Sentinel−1 IW single-pol. (VV) imagery Optical: Google Earth VHR imagery Other: long-term GNSS measurements	non-linear PS-InSAR; data analytics; PEKM and LSTM data fusion
Jiuzhaigou (China)	operational site monitoring (see Section 3.5)	Optical: Google Earth VHR and Sentinel−2 multispectral imagery, and UAV-based VHR aerial photographs Other: field evidence and auxiliary data from the heritage site administration	image interpretation, change detection, machine learning
Tuva Republic (Russia)	archaeological mapping (see Section 3.6)	SAR: C-band Sentinel−1 IW mode SAR dual-pol. (VV, VH) and L-band ALOS−2 PALSAR−2 Fine Beam dual-pol. (HH, HV) imagery Optical: UAV-based VHR aerial photographs, WorldView−2 multispectral imagery Other: field evidence and archaeological excavation, ground penetrating radar, and geomagnetic data	image interpretation, machine learning

monitoring in the Province of Rome in Italy, and in Wuhan in China; see Table 1). Finally, the SAR scenes and any derived InSAR products are geocoded to the map geometry and ingested into the GIS environment (e.g. ESRI ArcMap/ArcGIS, QGIS), where feature extraction, image classification, and archaeological interpretation take place. Time series post-processing, semi-automated analysis for surface height extraction or hotspot identification, and data fusion using advanced approaches are also carried out for some use-cases (e.g. for stability and urban development monitoring in Wuhan).

While the project focuses on SAR, it also investigates the complementarity with optical data from space-borne sensors and proximity remote sensing. Satellite optical imagery, either panchromatic, Red-Green-Blue (RGB) single layers or multispectral scenes including visible, NIR, and other channels, are mainly handled using specialist image processing and analysis software (e.g. ENVI), in the GIS environment and/or directly into Google Earth Pro. When applicable (e.g. for the Ostia-Portus area in Italy; Table 1), optical bands are pansharpened to the enhanced resolution of the panchromatic band, combined to derive true and false color composites (e.g. false-color IR combination: NIR, red, green), and/or used to estimate vegetation indices such as the Normalized Difference Vegetation Index (NDVI). These derived products are crucial to ease the subsequent archaeological interpretation of crop/soil marks, landscape, and morphological features. VHR optical imagery acquired using UAV platforms (e.g. for the Jiuzhaigou use-case in China; Table 1) are orthorectified and geocoded to map geometry, to enable their ingestion in the GIS environment and their combined interpretation with other geospatial layers. Data mining and machine learning methods, such as Support Vector Machine (SVM) supervised learning models, are subsequently exploited for advanced image processing, parameter retrieval through regression and land cover classification (e.g. for the Jiuzhaigou use-case in China, and sites in the Tuva Republic in Russia; Table 1).

Fieldwork at the different sites (when logistics and security allow) enables the collection of evidence on heritage asset presence, characteristics, condition, and any damage, as well as information on crop/vegetation type and status, to support satellite data interpretation and validation of EO-based evidence and observations.

3. Results and discussion

This section presents the key results and discussion for each of the six use-cases investigated, organized in dedicated sub-sections. A stronger emphasis and more detailed narration are provided for two of the use-cases (Sections 3.1 and 3.4), the research activities of which largely engaged the project team during the 2020–2022 period. On the other hand, initial results and observations are presented for the other four use-cases, with a view to the further development of their analysis and interpretation during the second half of the project lifetime.

3.1. Detection of buried archaeological features in the Ostia-Portus area

An initial investigation on the detectability of (semi-) buried archaeological features in SAR imagery, aided by the analysis of optical data, was performed across the Ostia-Portus archaeological area, located ~22 km west of Rome and 3–4 km inland from the Tyrrhenian Sea (Figure 1(a,b)). This use-case was aimed to test the capability of multi-band SAR data to detect archaeological features in part-vegetated landscapes with mixed land cover and land use, transitioning from the urban fabric of the capital Rome, toward coastal landforms of the Tiber River mouth.

The abandoned Roman cities of Ostia (modern Ostia Antica) and Portus were founded as ports of Rome, the capital of the Roman Empire: Ostia in the 4th century BCE (Zevi 1996), while Portus in the 1st –2nd centuries CE, during the empires of Claudius (who built a semi-circular harbor wharf) and Trajan (who created the still recognizable hexagonal dock; Figure 1(c)) (Keay et al. 2005). Both cities have many still-emerging monuments and buildings, especially Ostia, one of the world's largest archaeological sites. Their hinterlands are likewise extremely rich in natural landforms related to the evolution of the Tiber River and the Tyrrhenian coastline, as well as archaeological evidence dating back at least to the Eneolithic (5th millennia BCE) (Figure 1(a,b))

For this use-case, the analysis focused on two areas particularly abundant of buried features: (a) Capo Due Rami (Figure 1(c)), bounded by the Portus site to the west and the Tiber River course and Fiumicino artificial canal to the east and south, respectively. In this area, most of the archaeological evidence identified by remote sensing and geophysics is located along the pivotal *Via Portuensis* (connecting Rome to its harbor) and the Tiber, with numerous cultic, economic (e.g. warehouses) and funerary buildings, such as wealthy mausoleums. The interpretation of many features, however, remains hypothetical (Keay and Paroli 2011; Keay et al. 2020; Keay, Parcak, and Strutt 2014); and (b) Pianabella (Figure 1(d)), located southeast of Ostia Antica and, in Roman times, crisscrossed by an orthogonal network of roads where dense necropolises and wealthy residences overlooking the Tyrrhenian Sea developed. Only portions of the

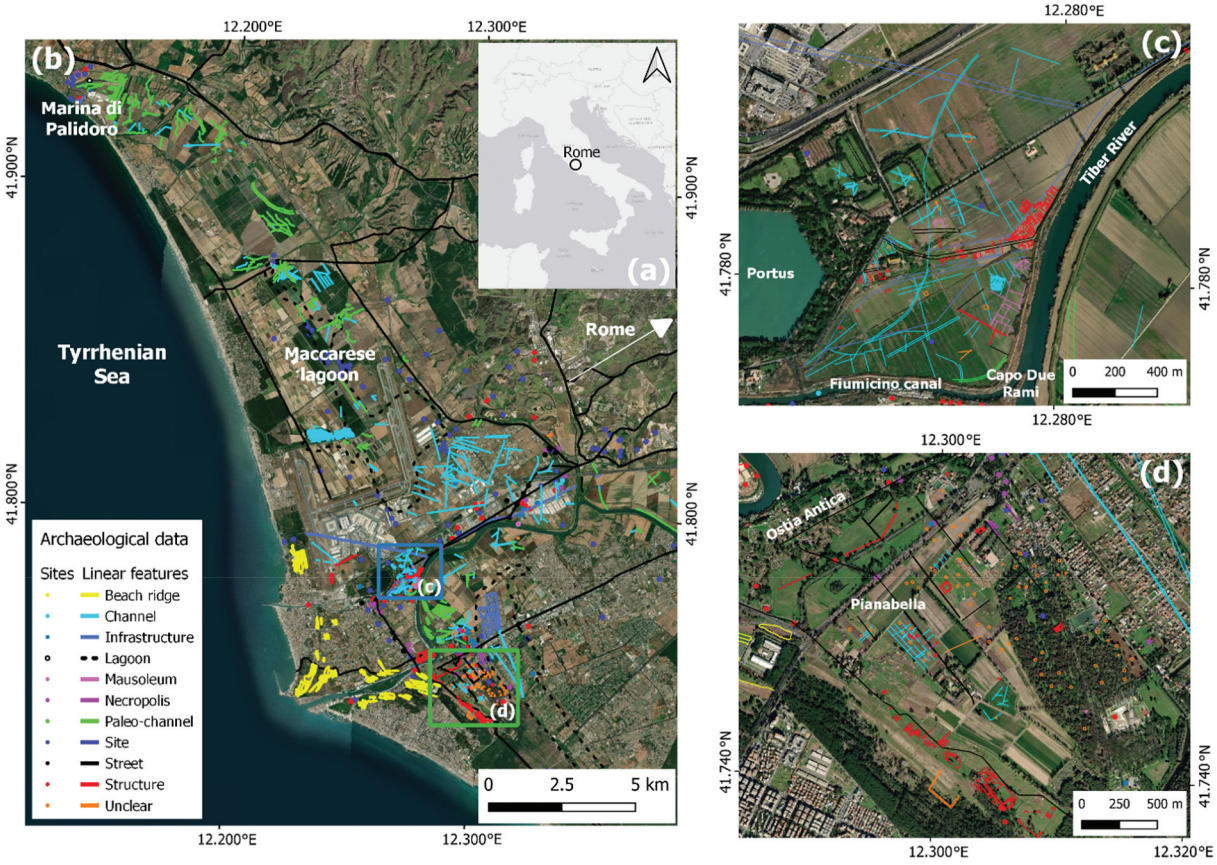

Figure 1. Overview of the Ostia-Portus study area in the province of Rome (Italy). (a) Geographic location in Italy; (b) archaeological mapping of sites and linear features, with zoomed views over the sectors known as (c) Capo Due Rami and (d) Pianabella. Data are overlapped onto ESRI base maps ©ESRI, DigitalGlobe, GeoEye, earthstar geographics, CNES/Airbus DS, USDA, USGS, AeroGRID, IGN, and GIS user community.

roads and nearby necropolises have been excavated yet, while the productive buildings (possible Roman farms) identified within the road network are primarily known from historical aerial photographs (Heinzelmann 1998).

Many archaeological features and geo-archaeological traces at these sites can be mapped by remote sensing through the detection of "crop marks", i.e. differences in vegetative growth due to variations in soil conditions caused by buried features. These marks can be "positive" when vegetation above the buried remains is more luxuriant due to the presence of negative features (e.g. canals and pits that are filled in and thus retain more water and nutrients than the surrounding soil), or "negative" when buried structures (e.g. building remains) hinder vegetation growth (Wilson 2000).

A systematic database was first generated (Figure 1(b)) to catalog crop and soil marks visible in historical aerial photographs of the National Archive of Aerial Photography – Central Institute for Cataloging and Documentation from 1911 to 1973 and the Italian Ministry of the Environment from 1988 to 2011, and in VHR satellite images (i.e. ESRI World Imagery, Google Earth and Microsoft Bing base maps, and 0.5 m resolution data acquired by SkySat, Pléiades and WorldView −2). The database includes both natural (e.g. paleo-channels, beach ridges) and anthropogenic (e.g. roads, necropolises, structures, channels) evidence, and was integrated with archaeological data from published literature and the Regional Landscape Plan of Lazio, to provide interpretation and/or chronology of each feature. In total, the database counts 1616 linear features (among which, 515 structures, 401 canals, 268 paleo-channels, 89 beach ridges, 87 streets, 58 mausoleums, and 48 necropolises) and 259 point-wise archaeological sites. Etruscan and Roman sites are known north of the Maccarese lagoon (Enei 2001), now reclaimed, along with dozens of fluvial paleo-channels of secondary streams. East and south of the lagoon, numerous pre- and protohistoric sites were discovered (De Castro et al. 2018), together with the remains of Roman salt pans (Morelli 2020) and several rural sites (Morelli 2014; Morelli et al. 2011). Abundant in buried buildings are also: Capo Due Rami (Figure 1(c)) and Isola Sacra (a stretch of land between Portus and Ostia), the areas north and east of Ostia Antica (where tens of scroll bars and dunes/swales were mapped, respectively), and Pianabella (Figure 1(d)), with numerous residential and funerary structures observed along the main ancient roads.

Multi-frequency SAR data collected in C-band by RADARSAT−2 Fine Beam and Sentinel−1 IW, X-band by COSMO-SkyMed, and L-band by ALOS−1 PALSAR

were first considered (see Table 1), pre-processed, calibrated, multi-looked and geocoded to map geometry. SAR image interpretation was aided by the analysis of a range of optical imagery acquired in 2017–2022, including HR data by Sentinel–2 (48 scenes, with 10 m resolution for visible and NIR channels, and 20 m for vegetation red edge and narrow NIR) and PlanetScope (121 scenes, with 3 m resolution), as well as the VHR data by SkySat, Pléiades and WorldView–2, and the Google Earth, ESRI and Bing base maps. In terms of temporal coverage, one Sentinel–2 image per month was considered in 2021–2022, with an enhanced revisit of 5 days during SAR acquisition campaigns. This regular observation was integrated with PlanetScope data offering almost daily coverage. SkySat, Pléiades, and WorldView–2 images were selected for the period May-September, considered as the most favorable for crop mark formation based on the analysis of existing aerial and satellite data. Validation of satellite observations was achieved using evidence collected in the field to identify vegetation status, ploughing/harvesting activity, and crop/soil marks visibility directly on the ground (see Table 1).

Differences in crop marks visibility at the different SAR bands (L, C, and X), resolutions (12 to 1 m) and polarizations (HH, HV, VV, VH) can be recognized when comparing the various image stacks (Figure 2). The analysis highlights a progressive increase in the detectability of smaller archaeological features when moving from L to X band, from co- to cross-polarizations, and toward finer spatial resolutions. In particular, it is apparent that with 1 m resolution imagery from COSMO-SkyMed Enhanced SpotLight (ES) mode, the analysis can be brought to the most suitable detail capable of robustly supporting archaeological mapping of the main linear features and structures

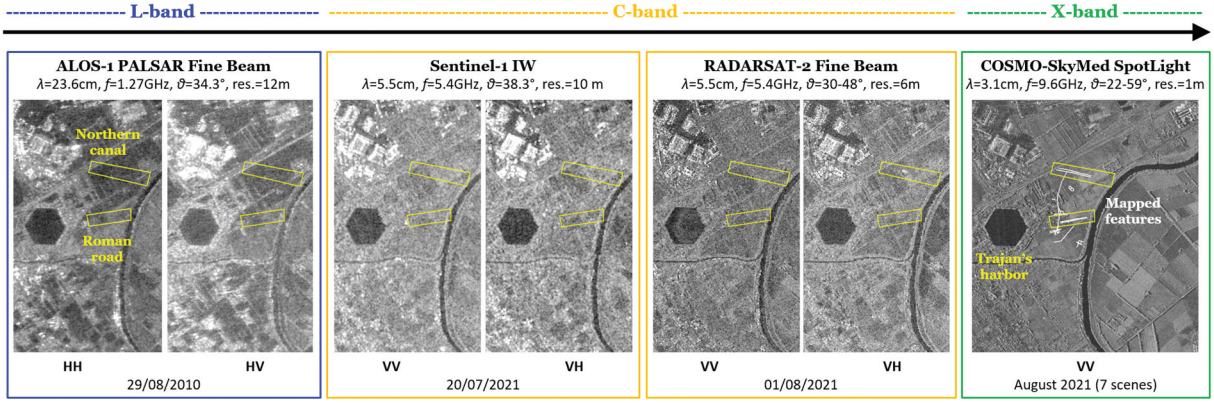

Figure 2. Comparison of SAR imaging bands, polarizations, and spatial resolutions over Portus and northern Isola Sacra (see location in Figure 1(c)), with the indication of main acquisition parameters and characteristics of each dataset. Credits: ALOS data ©JAXA/METI 2010, accessed through ASF DAAC; contains Copernicus Sentinel–1 2021 data; RADARSAT–2 data ©MDA Ltd. 2021, all rights reserved; RADARSAT is an official mark of the Canadian Space Agency; COSMO-SkyMed® products ©ASI 2021, all rights reserved.

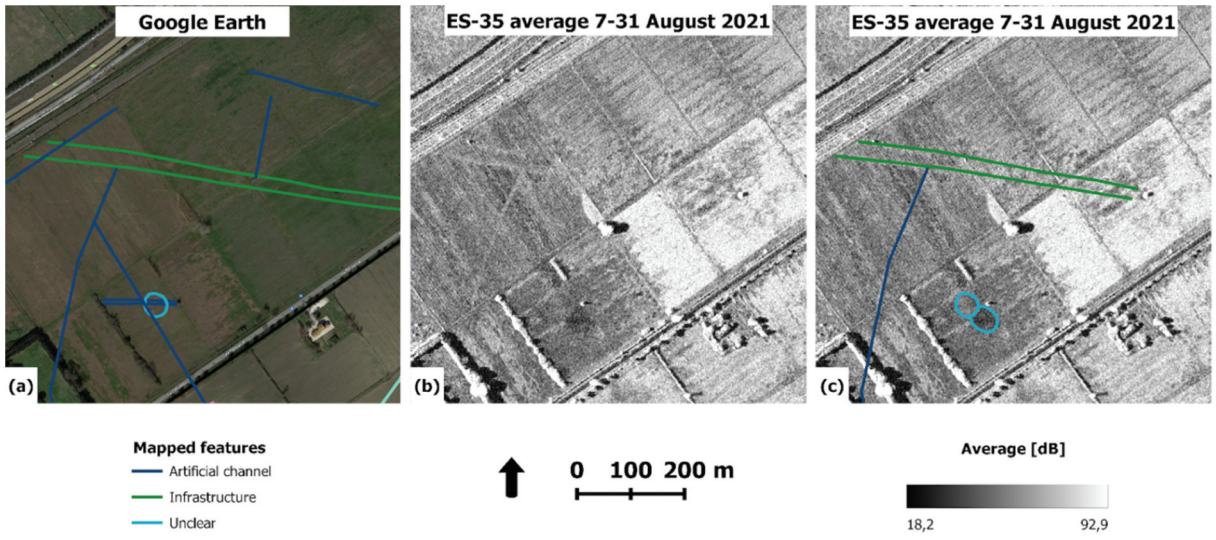

Figure 3. Example of integrated optical and SAR image interpretation in the area of the Northern Canal (green lines), northeast of Portus hexagonal basin. (a) Preliminary archaeological mapping onto Google Earth VHR base map, and (b) multi-temporal averaged COSMO-SkyMed Enhanced SpotLight SAR backscattering, with (c) archaeological interpretation. Credits: Google Earth image ©2022 Maxar Technologies; COSMO-SkyMed® products ©ASI 2021, all rights reserved.

that are shallow-buried across the landscape. An example lookup at the local scale of some crop marks detected by COSMO-SkyMed imagery is provided in Figure 3. Multi-temporal averaging of the SAR backscatter of 7 ES scenes acquired in August 2021 with ES −35 beam (59.19° incidence angle at scene center) and VV polarization along ascending orbits provides clear evidence of some vegetation marks that are correlated with the presence of the Northern Canal and other artificial channels, located northeast of Portus hexagonal basin (Trajan's harbor).

A total of 40 AOIs, including geo-archaeological features and neighboring areas where no crop marks were expected, were selected to conduct the multi-temporal analysis of spectral bands, profiles, and vegetation indices in the presence/absence of buried archaeological features, and to highlight any differences in vegetation status which could indicate crop marks due to yet unknown features.

At Capo Due Rami (Figure 4), similar spectral profiles and NDVI trends are recognizable at the buried *Via Portuensis* (AOI 8) and outside known features (AOI 18) between January and April 2021 (Figure 4(c-e)). Since 20 May 2021 (Figure 4(f), higher reflectance at 704 to 865 nm was recorded for AOI 8 due to a recent vegetation cut and freshly exposed soil. After this cut, vegetation grew back quicker on AOI 18 than on AOI 8, as visible in both spectral profiles and NDVI trends of 14 June and 29 July (Figure 4(g,h)). This is compatible with the typical behavior of soil without buried structures, compared to the location where very substantial building material related to the *Via Portuensis* Roman road lies underground, hindering plant growth, particularly during periods with limited rainfall as typically happens during the summer season in Rome. After mid-September, instead, vegetation regrowth was initially faster in AOI 8 (17 October) than in AOI 18 (31 December), as visible at 704 to 865 nm and in the NDVI profile, but this was likely due to differences in land use between the northern and southern halves of the field.

Opposite phenomena seem to characterize the "ovate feature" (AOI 3 in Figure 5(b)), referred to by Keay, Parcak, and Strutt (2014) as a possible amphitheater located inland of Portus (Figure 5(a,b)) but whose interpretation has not yet been confirmed by ground-truthing. This appears as an area of greater vegetative luxuriance (i.e. positive crop mark) than the surrounding soil. Similar spectral profiles are recognizable between January and April 2021 at both this feature and the reference location (AOI 4) (Figure 5(c, d)). On 20 May, a significant drop in plant presence was recorded due to a clear vegetation cut and freshly exposed soil, which only affected AOI 3, as visible in the spectral profiles and corresponding NDVI (Figure 5(e)). An identical NDVI drop occurred at AOI 4 on 14 June only, suggesting that the cut continued across the field after 20 May. More interesting is the subsequent vegetative regrowth that characterizes AOI 3 (Figure 5(h)), with a peak of NDVI in July (0.6) doubling AOI 4's one and being persistently higher throughout the following months, but progressively declining before it stabilized around 0.4 in October (Figure 5(e)). This NDVI behavior highlights

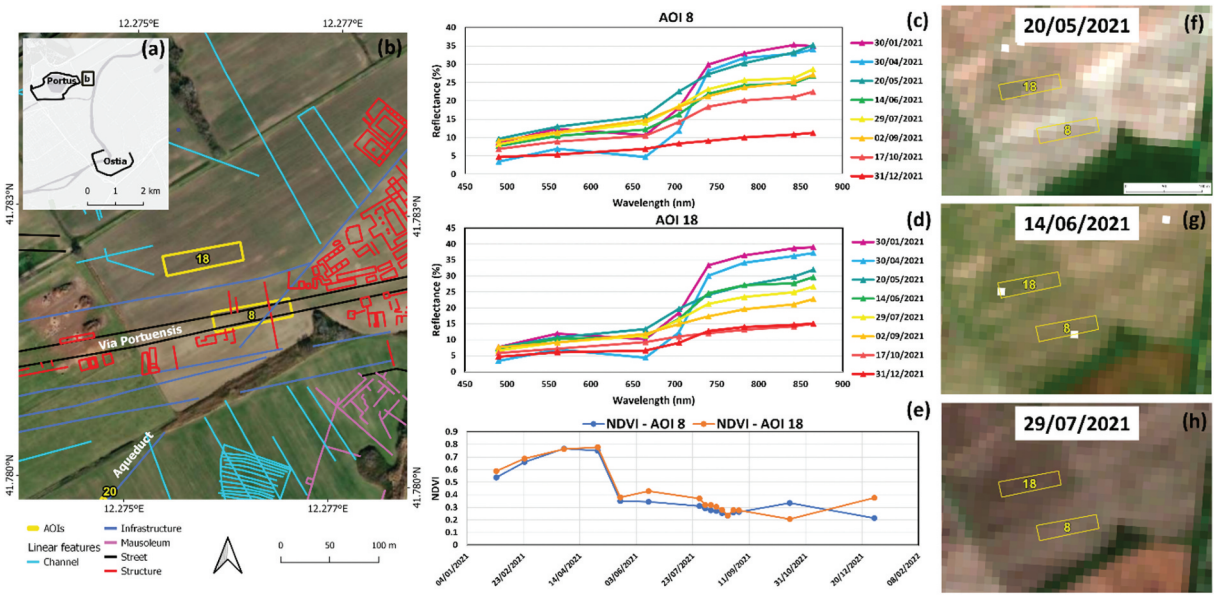

Figure 4. Spectral analysis of crop marks at the archaeological remains of Via Portuensis. (a) location within the Ostia-Portus site; (b) detailed mapping of known features, with identification of Via Portuensis (AOI 8) and the reference location (AOI 18) onto ESRI base map; Sentinel−2 spectra extracted for (c) AOI 8 and (d) AOI 18 during 2021; (e) NDVI temporal evolution of both the AOIs, and RGB color composites showing their land cover on (f) 20/05/2021; (g) 14/06/2021 and (h) 29/07/2021. ESRI base map ©ESRI, DigitalGlobe, GeoEye, earthstar geographics, CNES/Airbus DS, USDA, USGS, AeroGRID, IGN, and GIS user community. Contains Copernicus Sentinel−2 data 2021.

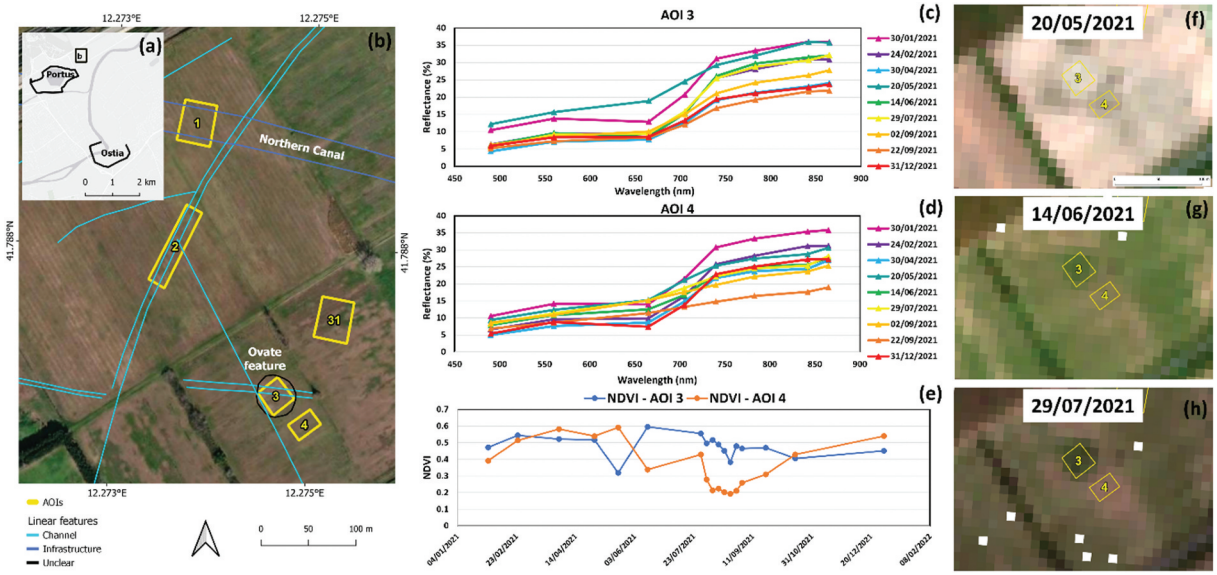

Figure 5. Spectral analysis of crop marks at the archaeological remains south of the Northern Canal. (a) Location within the Ostia-Portus site; (b) detailed mapping of known features, with identification of the ovate archaeological feature interpreted as a possible amphitheater (AOI 3) and the reference location (AOI 4) onto ESRI base map; Sentinel–2 spectra extracted for (c) AOI 3 and (d) AOI 4 during 2021; (e) NDVI temporal evolution of both the AOIs, and RGB color composites showing their land cover on (f) 20/05/2021; (g) 14/06/2021 and (h) 29/07/2021. ESRI base map ©ESRI, DigitalGlobe, GeoEye, earthstar geographics, CNES/Airbus DS, USDA, USGS, AeroGRID, IGN, and GIS user community. Contains Copernicus Sentinel–2 data 2021.

that AOI 3 feature was covered by luxuriant vegetation during most of the observation period (Figure 5(g,h)), even during summer, when rainfall was scarcer. Hence, should it be confirmed to be an amphitheater, the actual typology of the monument could explain this peculiar vegetation cycle, potentially caused by increased water and nutrient stagnation within the depressed central area, which is bounded externally by an 8 m wide double ring, the latter being at a slightly higher elevation (see, in this respect, the interpretation made by Keay, Parcak, and Strutt (2014) using a 1 m LiDAR DTM).

In Pianabella (Figure 6(a,b)), three AOIs within the same field were considered: AOI 13, above a large

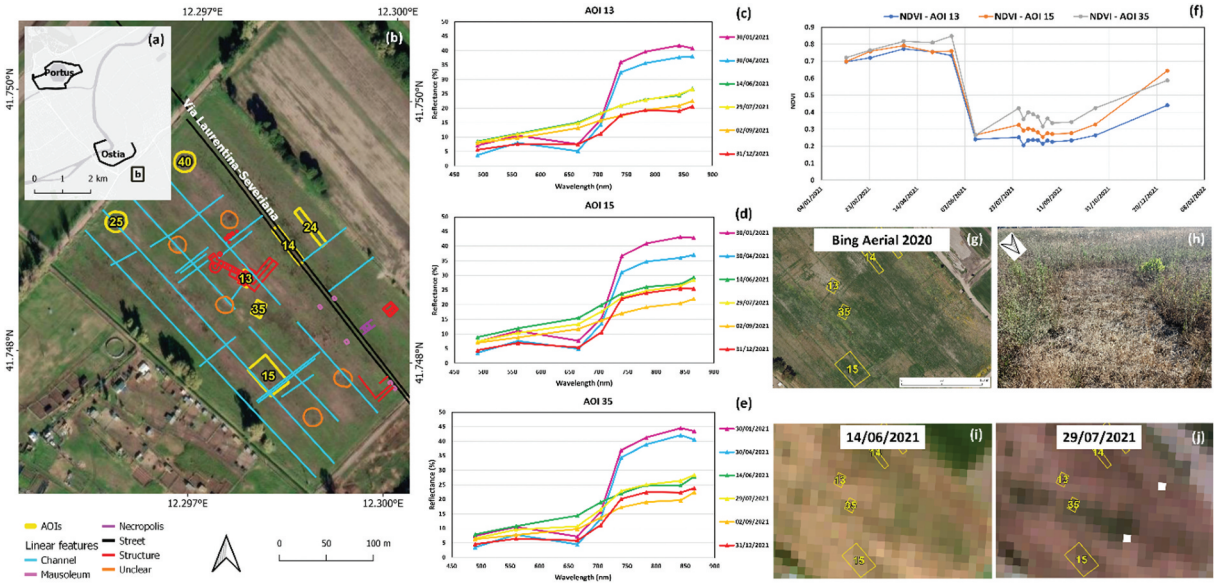

Figure 6. Spectral analysis of crop marks at the archaeological remains near Via Laurentina-Severiana, in Pianabella. (a) location within the Ostia-Portus site; (b) detailed mapping of known features, with identification of a large building with several internal rooms (AOI 13), channels (AOI 15) and the reference location (AOI 35) onto ESRI base map; Sentinel–2 spectra extracted for (c) AOI 13, (d) AOI 15 and (e) AOI 35 during 2021; (f) NDVI temporal evolution of the three AOIs; (g) crop marks identified onto Bing 2020 base map; (h) photograph of an internal room within AOI 13 with negative crop mark likely due to the buried thick floor (taken on 12 July 2022); and Sentinel–2 RGB color composites showing the land cover of all the fields on (i) 14/06/2021 and (j) 29/07/2021. ESRI base map ©ESRI, DigitalGlobe, GeoEye, earthstar geographics, CNES/Airbus DS, USDA, USGS, AeroGRID, IGN, and GIS user community; BingMaps ©2023 Microsoft – vexcel imaging. Contains Copernicus Sentinel–2 data 2021.

buried structure with several interior rooms recognizable both on satellite images and in the field (Figure 6(g,h)); AOI 15, with two positive crop marks interpretable as channels (perhaps not of ancient origin); and AOI 35, outside of any known feature. Historical observations through VHR optical images (e.g. Google Earth Pro 1 July 2019; Google Earth Pro 22 May 2020; SkySat 11 July 2022; Bing image collected during 2020) highlight the formation of a negative crop mark in the area of AOI 13, which therefore appears to be an ideal candidate feature for multi-temporal spectral analysis. During winter, spectral profiles and NDVI at the 3 AOIs are very much alike, while some slight but significant differences could be noted in summer, with spectral values at 704 to 865 nm slightly lower in AOI 13 compared to AOIs 15 and 35 (Figure 6(c-e)). Similarly, NDVI values are lower for AOI 13 (Figure 6(f)), where more difficult vegetative growth is expected due to the buried structures, compared to AOI 15 where the channels should favor vegetation growth due to greater water and nutrient retention (Figure 6(i)). Even higher is the NDVI at AOI 35, where the regrowth of wild plants is extremely fast but does not seem to be attributable to anthropogenic evidence (Figure 6(j)). The same trend also characterizes the early autumn months (i.e. September and October), suggesting that no particular anthropogenic activities took place across the whole land lot until vegetation levels started to rise back significantly by December.

3.2. Identification of subsidence threats to heritage assets in the province of Rome

In the wider Province of Rome (5363 km^2), the use-case focused on long-term InSAR ground deformation analysis with big data stacks of Sentinel–1 IW SAR imagery (see Table 1) to enable the estimation of present-day ground stability, and identification and characterization of surface deformation processes that may represent a potential threat to heritage assets.

As demonstrated by the wealth of scientific literature that has been published in the last two decades (e.g. Campolunghi et al. 2007; Delgado Blasco et al. 2019; Raspini et al. 2016; Stramondo et al. 2008), the study area of Rome is ideal for investigating these types of land surface processes and their interactions with anthropogenic activities and land cover land use. This is thanks to, at least, the following reasons: (i) geological and geomorphological characteristics of the valley, where the city and its hinterlands are located; (ii) the variability of such characteristics causing differential behaviors between and even within quarters, also in relation to the construction period and foundation types of the affected buildings and infrastructure; and (iii) the succession of several phases of building construction and city expansion over the centuries. With regard to the latter aspect, it is worth recalling that new sectors of urban development encompass those located at Ponte Galeria along the Tiber River and at Fiumicino airport, where former marshes and ponds were reclaimed between the end of the 19th and the early 20th centuries (Amenduni 1884). Not to forget, that the Province of Rome is home to a broad range of cultural heritage, that may be affected by ground instability: from the standing monuments and historical buildings within the UNESCO World Heritage Site (WHS) encompassing the whole historic center within the city walls at their widest extent in the 17th century, to the exposed archaeological remains and linear structures (e.g. aqueducts, ancient roads), as well as archaeological sites (e.g. Portus and ancient Ostia) and still buried remains, spread across suburban and rural landscapes of the wider province up to the coast.

Given the knowledge of the historical patterns of ground stability and land subsidence gathered through previous research based on ERS–1/2, ENVISAT, RADARSAT–1/2 (Tapete et al. 2012, 2015), and COSMO-SkyMed (Cigna et al. 2014) time series, the use-case was intentionally focused on the most recent Sentinel–1 observations only, and on massive InSAR processing.

The parallelized SBAS processing approach (Casu et al. 2014; Manunta et al. 2019), implemented into ESA's Geohazards Exploitation Platform (GEP) (Foumelis et al. 2019) and running by exploiting its HPC infrastructure, provided an overview of Line-of-Sight (LOS) ground displacement histories and rates in 2018–2022 for more than 460,700 coherent targets across the whole Latium region (17,242 km^2; Figure 7(a,b)). This was based on the processing of a stack of 124 Sentinel–1 scenes acquired along ascending mode track 117, one of the longest ever published over the city of Rome (87 scenes of the same track, albeit over a different period, were processed by Delgado Blasco et al. 2019).

Several hotspots showing significant land deformation (mainly indicating the occurrence of subsidence) were identified across the Province, such as in the area of Fiumicino International Airport and along the Tiber River alluvium (Figure 7(c,d)), involving monuments and heritage assets. The patterns in the area of Fiumicino airport and Ponte Galeria showing peak values of vertical velocity (V_v) ranging between −0.9 and −2.9 cm/year find a matching multi-temporal comparison with those retrieved by Delgado Blasco et al. (2019) based on Sentinel–1 2015–2018 data processed with SNAP-StaMPS PS-InSAR technique. Furthermore, the Sentinel–1 2018–2022 InSAR results exhibit a seamless continuity with ERS–1/2 (1992–2000) and RADARSAT–1 (2003–2007) deformation patterns and time series discussed by Raspini et al. (2016), ERS–1/2 (1992–2000), ENVISAT (2002–2010) and COSMO-SkyMed (2011–2015) integrated

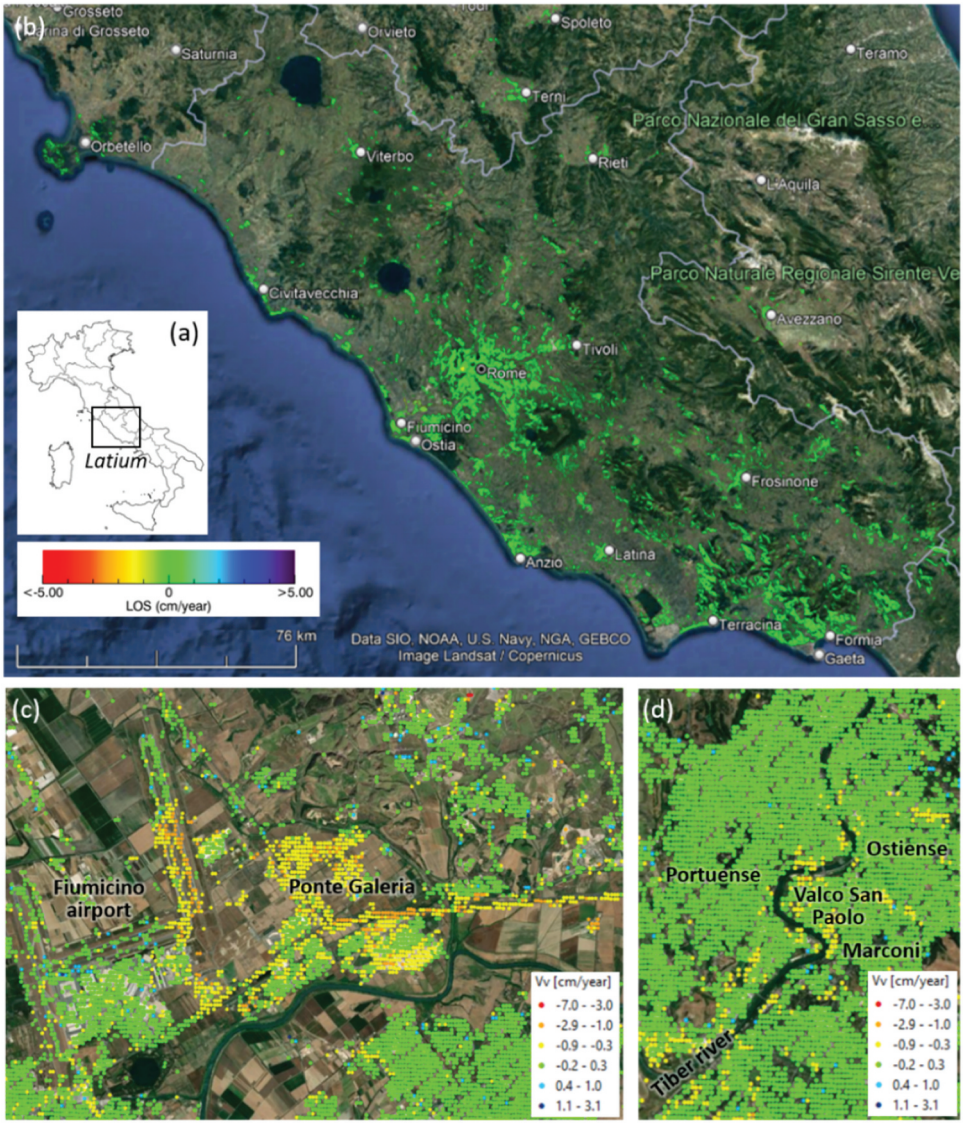

Figure 7. Multi-temporal InSAR analysis of ground deformation across the Latium region (Italy), using the parallelized SBAS method. (a) Geographic location; (b) Sentinel–1 LOS displacement rates in January 2018 – February 2022, with details of the derived vertical rates (V_v) for the areas of (c) Fiumicino airport and Ponte Galeria, and (d) the historic city center of Rome and the southern quarters Valco San Paolo, Marconi, and Ostiense. InSAR results in (b) are overlapped onto Google Earth VHR imagery ©2022 Maxar Technologies, while results in (c) and (d) onto ESRI base map ©ESRI, DigitalGlobe, GeoEye, earthstar geographics, CNES/Airbus DS, USDA, USGS, AeroGRID, IGN, and GIS user community.

by Bozzano et al. (2018), and COSMO-SkyMed (2011–2019) analyzed by Talledo et al. (2022). Accuracy assessment and evaluation of the impacts due to SAR wavelength, spatial resolution, and period analyzed are currently under investigation (and beyond the scope of the present paper).

Moreover, the patterns found in the present InSAR analysis agree with the published literature (Bozzano et al. 2018; Delgado Blasco et al. 2019) in marking the differential subsidence rates along airstrip number 3 of Fiumicino airport and between the three commercial sectors, i.e. Da Vinci shopping mall, CommerCity commercial center, and Rome Fair (Figure 7(c)). In the first case, the marked change in the subsidence rates along the NW – SE oriented airport runway is a direct surface manifestation of the abrupt lithological variation in the underlying geology (i.e. ~30 m thick body of highly compressible organic silty clay beneath the southern part of the runaway vs. low-compressibility silty sand below the northern part; Bozzano et al. 2018). In the second case, the higher V_v values observed over the CommerCity commercial center than over the Rome Fair buildings and Da Vinci shopping mall are plausibly explained by the combination of the effects due to building age, shallow vs. deep foundations, presence and thickness of low/high compressibility subsurface geological layers, as discussed in detail by Bozzano et al. (2018). This area is of particular interest for at least two reasons. First, it represents a relatively young phase of urban development and associated land conversion. The Copernicus Land Monitoring Service Urban Atlas 2006–2012 change layer produced in 2015 shows that all these sectors were converted from "Construction sites"

(CODE2006 13300) to "Industrial, commercial, public, military and private units" (CODE2012 12100) and, secondarily, to "Land without current use" (CODE2012 13300). Secondly, the CommerCity commercial center and Rome Fair are located just 4 km north-east of Capo Due Rami (see Section 3.1 and Figure 1(c)) along the *Via Portuensis*, which once connected Rome to its former harbor Portus, and now acts as one of the main roads of this commercial and service area. Therefore, this area may show what would be the manifestations of land subsidence, should new constructions were built onto similar geology in the nearby cultural landscape.

Spatially confined due to subsurface geology and interactions with urban development are also the land subsidence patterns distributed along the Tiber River course in the section crossing the southern quarters of the city of Rome, i.e. Portuense on the right bank and Valco San Paolo, Marconi and Ostiense on the left bank (Figure 7(d)). In addition to the well-known subsidence patterns within the UNESCO WHS, at Basilica Saint Paul Outside the Walls (Cigna et al. 2014) and Grotta Perfetta valley (Stramondo et al. 2008), Sentinel−1 InSAR results highlight a clear subsidence pattern with V_v up to −0.9 cm/year affecting the residential quarter of Valco San Paolo. Here, 19th and 20th-century heritage constructions testify an historical phase of the city, when infrastructure was also built for hydraulic management and improvement of the local sewage system (Miano et al. 2022). Likely, the observed deformation may have an impact on the conservation of this heritage, which only a more detailed InSAR analysis based on higher-resolution SAR data may unveil. In this perspective, Sentinel−1 cannot reach the level of definition required for structural health assessment at a single-building scale. However, the advantage achieved with the present Sentinel−1 time series analysis based on massive processing performed within GEP is the cost-effectiveness ratio between resource investment and knowledge return. Without the need to download and store heavy amounts of input data, use a proprietary or licensed InSAR processing software, and rely on in-house technical expertise to run the whole processing workflow, a first hotspot mapping exercise can be feasibly undertaken to identify and zone sectors of the city where cultural heritage may be affected by subsidence. Based on the retrieved evidence, it is then possible to evaluate whether a deeper investigation is needed. In this regard, the recently published study by Miano et al. (2022) based on full-resolution SBAS processing of COSMO-SkyMed data provides evidence that corroborates the validity of this multi-scale and multi-frequency approach.

Given the paucity of studies using multi-polarization datasets in InSAR deformation investigations, the performances of the SBAS InSAR chain using Sentinel −1 VV and VH cross-polarized channels were also trialed in the framework of the use-case (Figure 8). The experiment aims to identify the impact of the two polarizations in terms of the amount and quality of coherent targets that the method is capable to detect and track.

At equal conditions (namely, using the same input stack of 106 SAR scenes acquired along ascending track 117 in 2019–2021, the same processing area extent and thresholds), the analysis provided a total of ~ 456,000 coherent targets by processing the VV channel, and ~ 350,000 targets using the VH channel. This proved an increase of ~ 30% in the number of monitorable targets in VV with respect to VH, with clear benefits in suburban areas such as north of the Tiber River and along the runaways of Fiumicino airport (see red rectangles in Figure 8(a,b)). In these areas, the type of imaged surfaces, their orientation with respect to the satellite sensor, and their backscattering mechanism favored the identification of targets in the VV polarized scenes with respect to the VH ones. The imaged landscape and its features in the VH channel generally appeared with an overall lower SAR amplitude and temporal coherence, thus reducing the target identification rate across the suburban lands.

The specific characteristics of each imaging channel and the resulting target datasets will be accounted for during the interpretation of the estimated ground deformation to assess any further localized and wide area threats to the cultural heritage assets distributed across the Province, in addition to those already observed with the 2018–2022 analysis and discussed above. This activity will be the focus of future research on this use-case, in the next stages of the project.

3.3. Analysis of urban development and induced risk for cultural heritage in Wuhan

The goal of this use-case is the analysis of urban development in the city of Wuhan (China), to predict future encroachment on its heritage sites and identify endangered assets.

Wuhan is a young, fast-developing city located in the east of the Jianghan Plain and the middle reaches of the Yangtze River (Figure 9(a)). The confluence between the Yangtze River and its largest tributary, the Han River, spatially bounds the three main areas of the city, namely Hankou, Wuchang, and Hanyang, which are united into unique conglomerate since 1927.

Wuhan is an ancient city with a long history, dating back to the Neolithic era as early as 6000 years ago. Wuhan is the birthplace of the Jingchu culture, and has a large number of historical and cultural resources, with > 1300 historical sites, including ancient sites, tombs and buildings, modern historical sites and

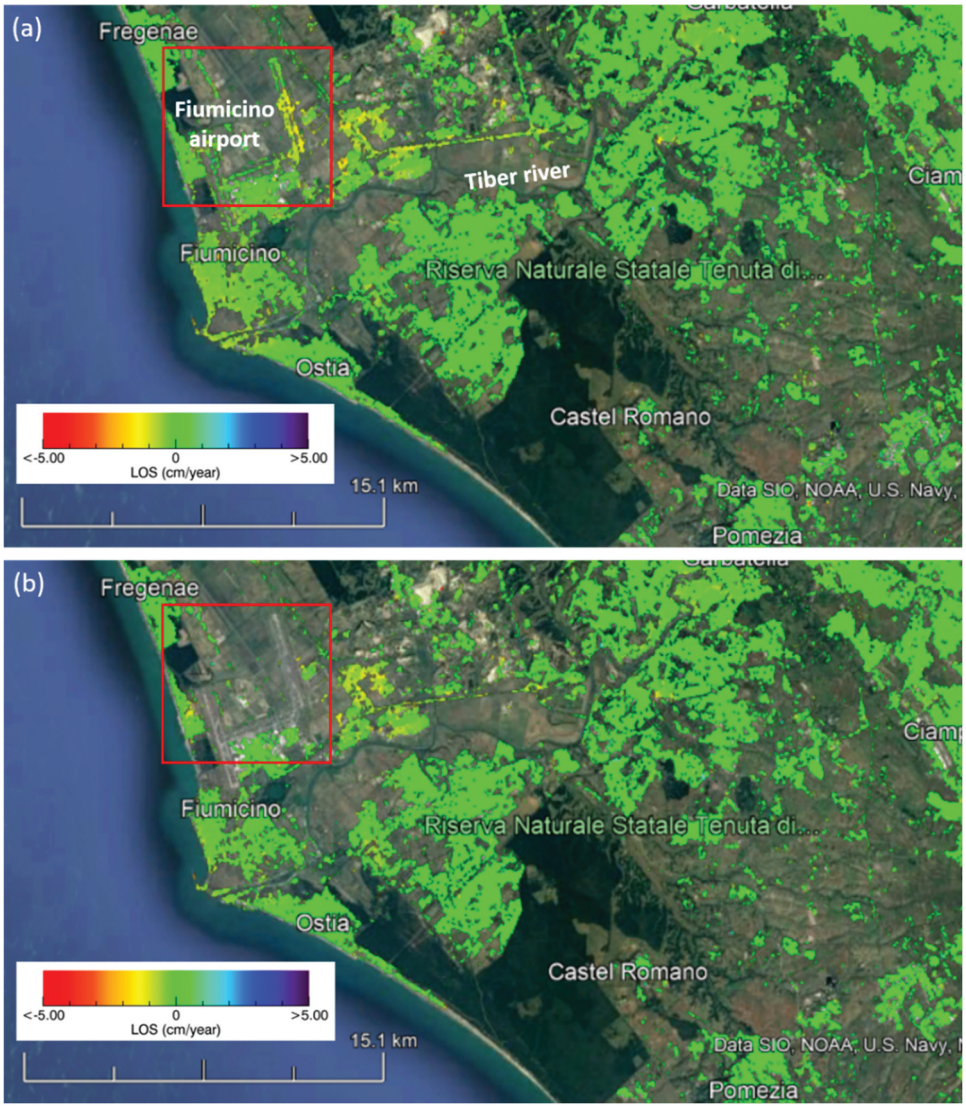

Figure 8. Comparison of the coverage of coherent targets obtained by processing Sentinel–1 IW (a) VV and (b) VH channels over the Province of Rome, overlapped onto Google Earth VHR imagery ©2022 Maxar Technologies. The red rectangle indicates an area where the difference in target coverage is very noticeable.

representative buildings, and stone inscriptions. Among the ancient relics, the sites from the Neolithic period (6000 years ago) to the Shang Dynasty (3000 years ago), the tombs of the Han (2300 years ago) and Ming (700 years ago) Dynasties, and the buildings of the Ming and Qing Dynasties (100 years ago) are particularly rich. They still retain famous historical buildings or relics such as the Ancient Qintai (1000 years ago), the Yellow Crane Tower (1800 years ago), and the Qingchuan Pavilion (500 years ago). The city also includes many areas of great cultural and historical significance related to recent history, such as the Wuchang uprising, sites from the Battle of Wuhan against Japanese invasion, and monuments of Sino-Soviet cooperation (e.g. the first bridge over the Yangtze River, constructed by Soviet engineers). Older sites from the colonial occupation can also be seen in Hankou, with several colonial buildings and cemeteries. Protecting these cultural heritage assets has not been a priority in the past in the framework of Wuhan's urban development, though this has changed in recent years, as heritage protection is becoming increasingly important and recognized.

The available historical information from declassified military intelligence photographs acquired by the KeyHole (KH) satellites allowed for manual mapping of the urban areas into the mid–1960s. Analysis of more recent urban development that occurred in the 2010s was then undertaken using a large stack of COSMO-SkyMed StripMap HIMAGE data with 396 images covering ~10 years. SAR image processing was based on the identification and analysis of Persistent Scatterers (PS) candidates across the investigated area.

PS points are generally defined to be "stable" over the complete observation period (namely, they are permanent/persistent reflectors). However, the analysis, in this case, focused on "temporarily" Permanent Scatterers (tPS) (Ferretti et al. 2004) due to the fast-developing city dynamics, while only a subset of PS

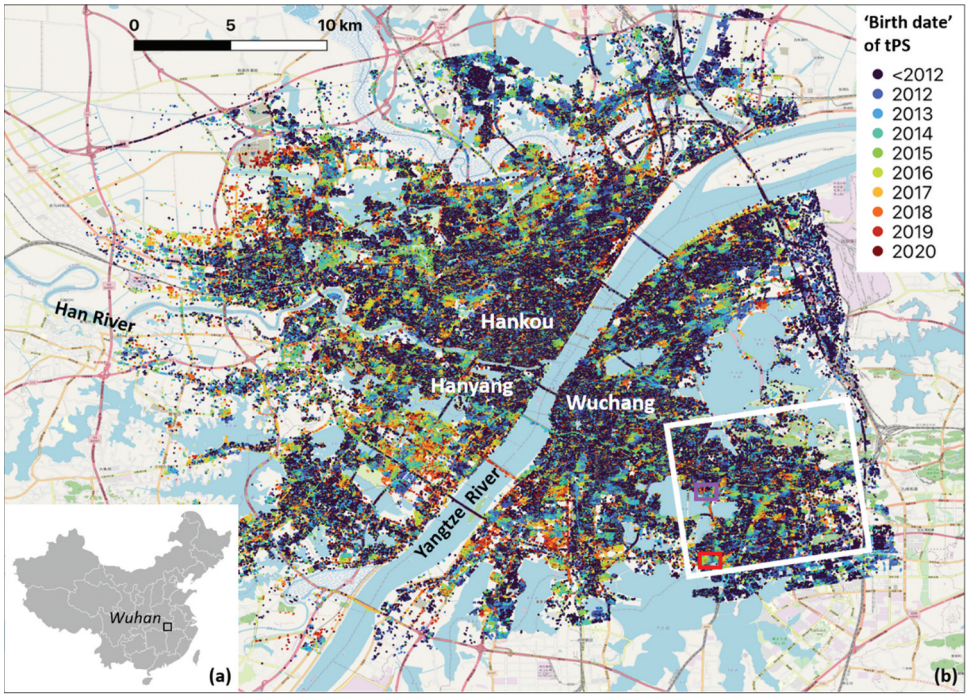

Figure 9. (a) The geographic location of Wuhan in China; and (b) map of tPS 'birth dates' based on dynamic PS-candidates detection and amplitude time-series analysis; the areas marked by the white, purple, and red rectangles are further investigated in Figure 10. The results in (b) are overlapped onto topographic map ©OpenStreetMap contributors.

Figure 10. Comparison of 2011 and 2020 Google Earth images for two areas within the Hongshan district in Wuhan (for location, see Figure 9). Credits: Google Earth images ©2022 Maxar Technologies.

points remained permanent over such a long period. To establish tPS, points that show a low amplitude dispersion index in a 30-image-long rolling window in time were considered. Points showing an index < 0.25 in any of the given time windows were included in the amplitude analysis. Based on the amplitude value of each of these points, the "birth date" and "death date" of each tPS (i.e. times when the PS appears and disappears, respectively) were established.

In Figure 9(b), the birth dates of the tPS over the area of Wuhan covered by the COSMO-SkyMed data stack are shown, providing a clear view of the urban development of Wuhan between 2012 and 2020. Several development areas can be observed in recent years. Besides growing outwards, a process of densification within the city can also be identified. An interesting trend in the last decade is the urban development close to and along the Yangtze River, and closer to several of the lake areas (green to dark red points in Figure 9(b)). Among the observed developments, it is worth noting the Yangtze riversides, which were off-limits for large urban developments

before, due to regular flooding events. After the construction of the Three Gorges Dam in the Yiling District in 1994–2008, the flood management significantly improved thus allowing now for more construction works along the riversides. As shown in Figure 10, many areas underwent significant development, including new landscaping of riversides and new engineering constructions (both private housing blocks and commercial units, low and high-rise buildings).

Long-term remote sensing observation with SAR is enabling the analysis of the urban development of Wuhan with unprecedented temporal granularity. SAR imagery proves particularly useful for such type of application, as SAR reacts strongly to man-made objects and allows for good separation between urban and non-urban areas. The approach tested in this use-case and based on tPS is just one possible approach to address the research goal. Since it requires long series of SAR observations as input, it is currently limited to areas where long data stacks are available. For instance, it is globally useable with Sentinel–1 data for analyzing urban developments from 2015 onwards in many other metropolises worldwide.

Future research will also focus on integrating "horizontal development" information (i.e. urban expansion) with "vertical development" observations (i.e. vertical growth of urban structures and buildings), to enable a 3D development analysis of the urban area and therefore a better risk assessment for cultural heritage sites in Wuhan. Structure heights and their changes will be estimated for PS and tPS points via multi-baseline InSAR. The technical challenge to address for such an application will be mainly due to the position of the identified PS and tPS. Indeed, most scatterers are typically identified on building façades and on the ground (see, for example, the study on ancient aqueducts by Tapete et al. 2015), while generally, few points are to be found on building roofs, therefore leading to sparser point distributions on high-rise buildings (where height estimations would be crucial to assess vertical development). Moreover, points located on building roofs, especially in high-rise buildings, may suffer from more motion (e.g. due to temperature and wind-related effects), thus adding further variables to the data processing and influencing PS identification and monitoring.

3.4. Ground deformation risk estimation for cultural heritage sites in Wuhan

A further research goal for the Wuhan use-case is focused on long-term ground stability monitoring and identification of any threats to cultural heritage deriving from land subsidence across the core of the city. To this aim, the regional and local geological setting of the ground onto which the city has been developed and the wealth of engineering works and new construction projects being undertaken over the last decades, play a key role in determining the main predisposing and triggering factors for land compaction. This process combines both natural and anthropogenic causes, and develops through a complex spatiotemporal behavior, as observed through past investigations by the authors (Tapete et al. 2021a).

As shown in Figure 11(a), the geological setting of Wuhan highlights that most of the Hankou area is built onto a Quaternary alluvial plain formed by flooding and siltation, with silty soft soils distributed widely (Chen, Chen, and Wu 2015). Carbonate rocks in Wuhan cover 1100 km^2, accounting for ~ 13% of the urban area, and they consist of six bands (e.g. Luo 2014). As the city economy develops and population increases, many buildings and much critical infrastructure (e.g. transport, private and public housing) are being constructed, thus boosting the water demand for residents and, in turn, groundwater

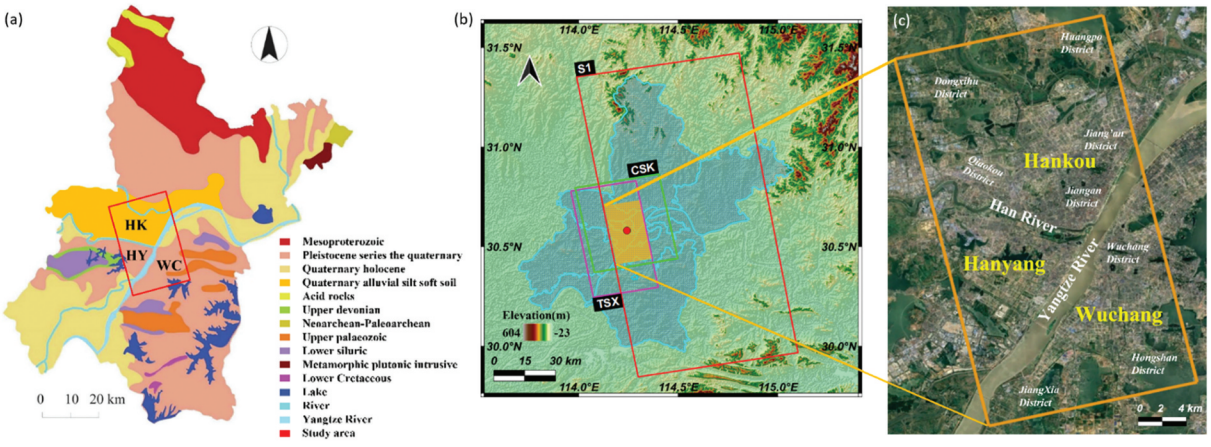

Figure 11. (a) Simplified surface geology of Wuhan after (Wu et al. 2020), with the indication of the study area (red rectangle) and the centers of Hankou (HK), Wuchang (WC) and Hanyang (HY); (b) Footprints of the Sentinel–1 (S1), TerraSAR-X (TSX) and COSMO-SkyMed (CSK) SAR data stacks, and (c) satellite image overview of the study area used for the InSAR analysis. Figure (a) is reproduced from Jiang et al. (2021), while (b) and (c) are from Jiang et al. (2023).

pumping from local aquifers. The combination of various natural and human factors has gradually led to a process of land subsidence across different sectors of the city, as observed by several previous studies based on satellite InSAR methods (e.g. Bai et al. 2016; Benattou, Balz, and Liao 2018; Zhou et al. 2017).

To monitor the long-term subsidence process affecting the city over the last decade and reveal its spatiotemporal variations, 286 X-band COSMO-SkyMed StripMap HIMAGE HH-polarized scenes acquired in ascending mode at 3 m resolution between 16 June 2012 and 3 November 2019 were exploited. This long data stack was collected via WUHAN-CSK – a research collaboration project between ASI and Wuhan University – and was processed using a non-linear PS-InSAR method, as detailed by Jiang et al. (2021). Experiments focused on time series fusion were also undertaken using three ascending mode SAR datasets: (i) 89 COSMO-SkyMed scenes acquired in 29/05/2011–26/12/2015 (i.e. a subset of the longer stack processed with the non-linear method); (ii) 51 X-band TerraSAR-X StripMap HH-polarized scenes acquired in 14/01/2015–14/12/2018; and (iii) 30 C-band Sentinel−1 VV-polarized scenes acquired in 13/06/2019–27/04/2021.

After advanced multi-temporal InSAR processing of each of the three SAR data stacks with the PS-InSAR method, the three output datasets were fused into a unique long series, by employing the Power Exponential Knothe Model (PEKM; e.g. Chen et al. 2018) and Long Short-Term Memory (LSTM; e.g. Qu, Yang, and Chang 2019) methods. This enabled the fusion of the series through the 1 year-long data overlap between the COSMO-SkyMed and TerraSAR-X datasets and across the 6 month-long temporal gap between TerraSAR-X and Sentinel−1 data. For the overlapping regions, the deformation curves of COSMO-SkyMed and TerraSAR-X were first modeled using the PEKM method, and then the fusion point was determined using the minimum gradient method. The fused results were then further processed with the LSTM neural network to predict the gap between TerraSAR-X and Sentinel−1 displacement records, to obtain a unique and complete long-time sequence covering the whole 2011 to 2021 period. Full technical details about the fusion approach and the methodological workflow are available in Jiang et al. (2023).

The SRTM DSM, Google Earth VHR optical images, and geological and precipitation data from the administrative department of Wuhan's municipal government were also used to support the geospatial analysis and the InSAR data interpretation.

In the Hankou area, significant subsidence rates were detected (Figure 12(a)), with cumulative displacements reaching −150 mm in 2011–2021. This is the effect of land reclamation and artificial filling of the former lakes to expand the built-up area for rapid development, and the consequent long-term consolidation of the silt and soft soil foundation. According to the geological literature, the silty soft soil layer reaches a thickness of >5 m under the Hankou area (see Figure 11(a) for location and geology). Although the process of soft soil consolidation is well-known in this area, the degree of consolidation of soft soils had not yet been quantified. By assuming that all soft soil layers in this area are horizontally continuous with constant applied load and only vertical displacement occurs, and by excluding other factors, soft soil deformation is the only process ongoing. Using a hyperbolic model based on Terzaghi's one-dimensional consolidation theory, the final deformation and thus the consolidation degree can be calculated in each

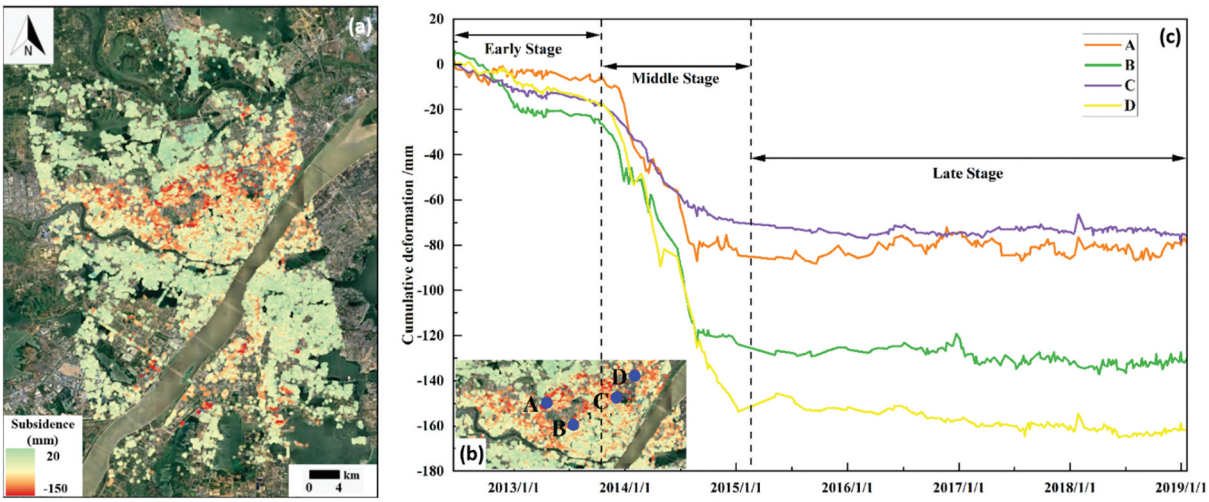

Figure 12. (a) Cumulative land subsidence map of Wuhan in 2011–2021 after InSAR time series data fusion, overlapped onto Google Earth imagery, with (b) detailed zoom over the area of Hankou, with the indication of the selected points A, B, C, and D in blue; (c) Comparison of the deformation curves of A, B, C, and D obtained from the non-linear PS-InSAR processing, with identification of the early, middle, and late stages of soil consolidation and compression. Figure (c) is reproduced from Jiang et al. (2021).

Table 2. Final land deformation and consolidation degree of the four selected PS points A, B, C, and D located within the Houhu area in Hankou, Wuhan (see Figure 12(b,c) for location and deformation curves, respectively). Data are reproduced from Jiang et al. (2021).

		Consolidation Degree of Soft Soil (%)						
PS Point	Final Deformation (mm)	2012	2013	2014	2015	2016	2017	2018
A	−90.8	3.77	6.28	74.31	88.83	91.11	92.22	95.66
B	−139.4	3.56	17.12	68.95	89.63	90.93	93.10	94.67
C	−80.0	7.37	18.56	69.36	89.24	89.68	89.74	90.67
D	−167.0	1.47	8.40	62.90	90.01	92.15	95.03	96.68

period (Figure 12(b,c)), as per the methodological approach presented by Jiang et al. (2021).

Four reference points were selected for validation and to quantify the degree of soft soil consolidation in the Houhu area in Hankou (Table 2). The average degree of consolidation of the four selected points was estimated to be <10% in 2012, while it increased significantly to > 60% in 2014. After a period of rapid consolidation, the degree reached >88% in 2015, after which it steadily increased at a rate of 1–2% per year and approached 100% in the final stage of the observation period. During this latter phase, the study area was generally stable and the possibility of settlement collapse was reduced (Jiang et al. 2021). These observations can be also contextualized in the framework of other anthropogenic factors, such as groundwater management practices. As observed by Costantini et al. (2016), some piezometric wells in Houhu recorded sharp groundwater declines as high as 5 m between mid–2013 and mid–2014, which may also explain the significant acceleration in the consolidation process during that period.

Further development of the ground deformation monitoring analysis will include the processing of historical SAR imagery acquired in the 1990s–2000s by the ERS–1/2 and ENVISAT missions. However, ESA's data archive highlights that the ERS–1/2 and ENVISAT stacks available for Wuhan are quite limited (<20 images each, with several temporal gaps), thus not ensuring a regular temporal sampling and therefore a good potential to extract robust PS-InSAR processing outputs of suitable precision.

The next research steps will also focus on exploiting the long-term and fused InSAR series to identify the main land subsidence threats to the cultural heritage of the city and characterize the spatial extent, magnitude, and trends of the ongoing deformation processes in proximity to key monuments and other heritage assets. Any damage already caused to such assets will be recorded, and the potential future impacts of the land deformation process will be assessed, should the process continue with such rates in the upcoming years.

3.5. Post-disaster monitoring and conservation of the Jiuzhaigou UNESCO Heritage Site

The Jiuzhaigou UNESCO natural WHS is located in the north-eastern Tibetan Plateau, in the topographic transition zone from the Tibetan Plateau to the Sichuan Basin in China (Guo et al. 2000). Landforms at the site are characterized by deep-incision gullies and high mountains with slopes > 30° (Figure 13), which make the use of remote sensing and other survey methods in the valley very challenging. The

Figure 13. UAV-derived aerial view of the sparking lake north-east of Shuzheng (103°54′00″ E, 33°12′20″ N), within the Jiuzhaigou UNESCO natural WHS in Sichuan (China), after the occurrence of the August 2017 earthquake.

maximum peak is >4700 m, while the minimum elevation is ~1200 m (Fan et al. 2018; Guo et al. 2021). On 8 August 2017, an Ms7.0 earthquake occurred in Jiuzhaigou County, Aba Autonomous Prefecture, in the Sichuan Province. Due to the high magnitude, shallow source, and high intensity of the earthquake, as well as the fragile geological environment of the valley, the event triggered thousands of landslides (Dong et al. 2020; Wu et al. 2018), the monitoring and characterization of which are essential and urgent for WHS protection and management.

To this aim, the team used pre- and post-seismic Sentinel−2 (10 m), post-seismic aerial (1 m and 0.16 m), and a series of Google Earth pre-seismic (about 0.5–1 m) images to identify landslides and establish a multi-temporal post-seismic landslide dataset. The post-seismic ortho-level image was acquired on 10 June 2020 using a CW −15 long-endurance full electric vertical take-off and landing fixed-wing UAV system, the operation of which was very challenging due to the steep valley, which can cause GNSS interruptions and falling winds, both significantly endangering UAV operations and safe flight.

Landslide identification was based on automated classification with SVM, as well as visual interpretation and field investigation, to ensure a complete landslide inventory. Additionally, the fundamental influencing factors of landslides were analyzed for an improved landslide susceptibility analysis to enhance future WHS protection and management efforts.

The results for 2017–2019 and 2019–2020 show that > 80% of the 2017–2019 post-seismic landslides are distributed within 200 m around the 2017 co-seismic landslide area, suggesting that the original landslide expansion is the primary source of landslides after the Jiuzhaigou earthquake, as can be seen in Figure 14 with the example of the Shuzheng landslide. Furthermore, the results show that the probability of new single landslides occurring far away from the original landslides reduces with time. The distance from the original landslide is also considered a reasonable index to quantify the legacy effect of the original landslide.

Landslide susceptibility appears mainly affected by earthquake-related factors. However, over time, in the years after the earthquake, this situation changes gradually to other influencing factors, such as the presence of deposits and the occurrence of rainfall. Therefore, the distance to the seismogenic fault is the most important factor influencing the distribution of co-seismic landslides. Unstable slopes caused by the earthquake have intense activities in the post-seismic initial stage, gradually changing from dangerous to relatively stable with time, and the activities are weakened. Thus, the slopes which strongly correlate with seismic factors decrease, and the high landslide susceptibility area is reduced. However, the deposits caused by the former co-seismic landslides accumulate along the slopes and generate post-seismic landslides in the form of the original landslide expansion, triggered by rainfall.

The analysis of multi-temporal sequences of satellite and aerial images over the WHS enabled the identification of the immediate and long-term impacts of the August 2017 earthquake on natural heritage assets, and the assessment of the time needed for the ecosystem to recover after the disaster and reach a new equilibrium (Figure 15).

These results provide useful inputs to support monitoring, management, and protection strategies at the WHS. Since post-seismic landslide susceptibility is mainly influenced by the spatiotemporal distance to existing landslides, post-seismic landslide prevention should focus on the expansion of original landslides, especially the large landslides that can be further triggered by rainfall. Moreover, the landslide deposits should be cleaned in time and the debris flows should be reasonably dredged to avoid secondary geological disasters.

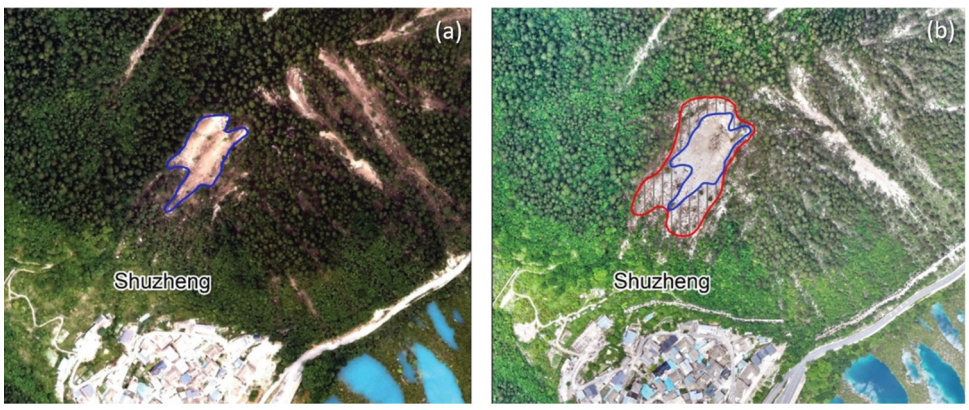

Figure 14. Example of post-seismic landslides: identification of the Shuzheng landslide edge in (a) 2017 marked in blue, and (b) 2020 marked in red, overlapped onto aerial imagery.

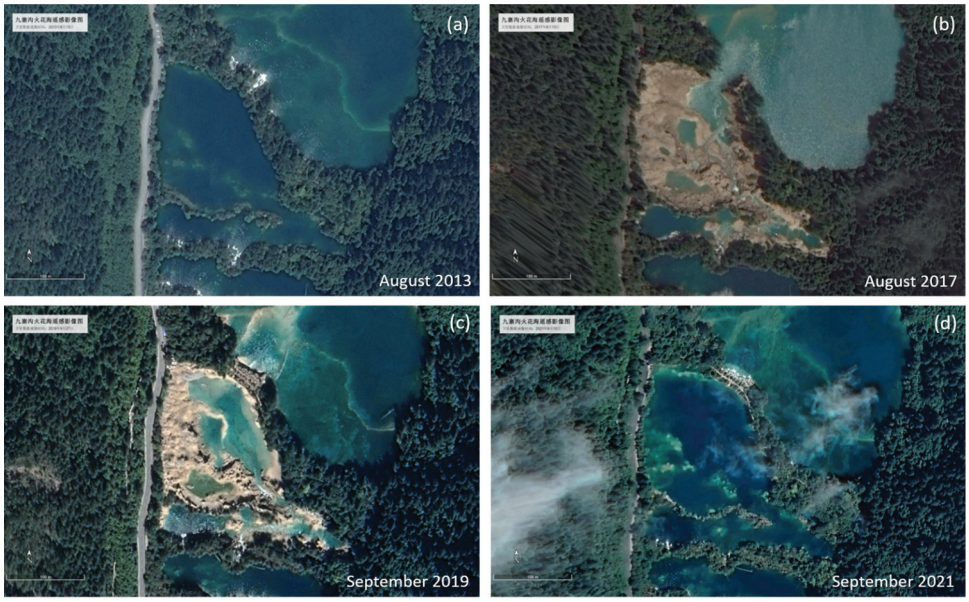

Figure 15. The multi-temporal sequence of Google Earth VHR images of the area of the sparkling lake near Shuzheng, showing the (a) pre-event and (b-d) post-event scenario related to the August 2017 earthquake. Credits: Google Earth (a), (c-d) images ©2022 CNES/Airbus, and (b) image ©2022 Maxar Technologies.

Although using remote sensing in this extreme mountainous area proved very challenging, field observations were even more difficult to conduct in this environment. Some landslide sites were unreachable when considering safety standards for scientific work. Therefore, remote sensing acted as an invaluable tool for landslide monitoring and WHS protection.

3.6. Detection of burial mounds in the Siberian valley of the kings

Detecting, prospecting, and monitoring burial mounds ("kurgans") are among the main scientific goals of the use-case in the Uyuk River Valley (i.e. the Siberian Valley of the Kings), located in the Tuva Republic in Russia.

The "Tunnug 1" site was first discovered to be a highly significant Early Iron age site during a summer survey in 2017 (Caspari et al. 2018). The team used various remotely sensed datasets including WorldView–2 imagery, aerial photographs, 3D models, and DEMs to document an internal radial structure similar to the widely referenced "Arzhan 1" burial mound (Caspari et al. 2019). The site's location in the floodplain of the Uyuk Valley led to the formation of hypotheses about hydrological changes in the area shortly after the burial mound had been constructed. Subsequent excavations, however, revealed that the site had been used as a focal point of ritual funerary activity for over 2500 years (Figures 16 and 17), from the Bronze Age to the Turkic period (Chan et al. 2022; Milella et al. 2021; Sadykov et al. 2021; Sadykov, Caspari, and Blochin 2020). Additional surveys using

Figure 16. Excavations in the southern periphery of the 'Tunnug 1' burial mound revealed funerary structures dating to the 2nd – 4th century CE (93°32′50″ E, 52°00′25″ N) in Tuva Republic, Russia. Photograph credits: Trevor Wallace.

Figure 17. UAV-derived aerial view of a unique wooden structure that was identified underneath the 'Tunnug 1' tomb; dendrochronology samples have been obtained. Image credits: Jegor blochin.

optical and SAR data showed the burial mound to be an isolated occurrence in a wetland zone (Caspari et al. 2020). Well-preserved organic remains including wooden logs from larch trees, allowed for a precise dating of the site to between 833 and 800 BCE (Caspari et al. 2020). This makes the burial mound comparable to the "Arzhan 1" site in terms of size and chronological position at the beginning of the Early Iron Age in the Eurasian steppes. The abundance of the wooden construction material (larch trees) makes the burial mound likely contemporary with the harvesting from local forests and reduces the likelihood of old wood effects.

Despite travel restrictions related to the ongoing COVID−19 pandemic in 2019–2021, archaeological investigations progressed, with an excavation campaign carried out in conjunction with remote sensing monitoring using Sentinel−1 SAR data supported by UAV surveying including the collection of optical data and aerial magnetometry. Data are currently being processed with standard image interpretation approaches and advanced machine learning algorithms. A stone wall surrounding the monument, which seems to contain deep pits underneath was identified. This is a promising finding because early Scythian monuments often feature additional burials at the edge of the main burial mound. For the first time, an artifact decorated in Scythian animal style displaying raptor heads was found (the use of such artifacts has yet to be clarified). Within the stone layer, several unique stone stelae were identified. These do not belong to any currently known and well-defined type of stelae, requiring further research.

The initial observations based on satellite data and field research at the "Tunnug 1" site have contributed to opening up a new understanding of one of the most important burial mounds in the Eurasian steppes. A similar approach will be applied to other sites also with regard to detecting and monitoring anthropogenic impacts on burial mounds (see Caspari 2018). Unfortunately, as of today, almost all "royal" mounds have been impacted by severe looting and/or agricultural activities. Due to the relative remoteness of many of these heritage sites, monitoring efforts have to be remote sensing-based. Further work on this use-case will also focus on improving monitoring methodologies with respect to climatological factors. This is an important aspect, as some of the most valuable burial mounds are to be found in or close to permafrost areas (allowing for the preservation of organics). Global warming and thawing of permafrost endanger the organic remains in some of the sites in question that are currently still frozen and therefore extremely valuable for archaeological analysis. Learning more about the current extent of permafrost, monitoring spatial changes, and being able to predict the spatiotemporal patterns of future changes are of crucial importance for the planning and prioritization of future archaeological excavations.

4. Conclusions

In the framework of the 5th phase of the Dragon cooperation program, the SARchaeology project relies on the synergistic integration of SAR imaging, InSAR processing, archaeological science, and cultural heritage conservation expertise, made available by a multidisciplinary Sino-European team, to promote the exploitation of satellite SAR technologies, and advance the current state-of-the-art of data analysis techniques to address a broad range of applications, matching with both scientific research interests and daily practice duties. In providing an overview of the project achievements at the mid-term stage of the Dragon–5 cooperation, the use-cases presented and discussed in this paper allow for outlining the following conclusions and future perspectives:

- The increasing availability of multi-frequency SAR data collected by different sensors, from either past or current missions, is pivotal to compare different acquisition parameters (e.g. wavelengths, spatial and temporal resolutions) and support an experimental exercise to understand how to exploit SAR imaging mechanisms for archaeological prospection in areas that, due to their land cover and vegetation, are in general considered more challenging for crop mark detection with SAR.
- This objective can be also achieved by exploiting multi-temporal datasets to improve the commonly used approach based on spot (aerial) observations only, according to a multi-sensor SAR and optical paradigm. Frequently, crop marks are recurrent features across the landscape and their temporal behavior can be effectively monitored and characterized even at HR, e.g. with the use of Sentinel–2 time series.
- While the multi-temporal component is an established concept in InSAR-based studies of geological and anthropogenic hazards potentially affecting cultural heritage in urban areas, and the methods exploited for surface deformation investigation align with a well-known body of literature, the new perspectives relate to those coming from the experimentation of new analytical methods and the use of HPC and cloud computing facilities. Understanding the impact of SAR polarization (e.g. VV with respect to VH for Sentinel–1 data) on the number of deformation measurements that can be extracted will allow a more informed decision about how to select SAR input data, and the opportunities to exploit this additional information (or, on the contrary, to discard it), e.g. in land subsidence studies. The trials on using the height of extracted tPS as a proxy to map areas of urban expansion and densification, and thus identify city sectors where cultural heritage assets may be impacted, corroborate the hypothesis that not all the information stored in SAR data is currently utilized at its maximum potential and, instead, may be valuable and informative.
- When the physiographic characteristics of the environment to explore and monitor are challenging, it is even more recommendable the integrated use of satellite SAR and optical observations with proximity sensing, e.g. through UAVs. The experimentation on co- and post-seismic landslides affecting natural heritage sites proves how these technologies and data can support not only impact assessment due to a specific disaster event, but also better characterization of influencing factors and, thus, inform post-disaster and longer-term site management activities.

Additional use-cases within this research remit will be investigated. They will encompass paleo-channels and paleo-environments in Lop-Nor (China), Bronze Age cemeteries and other structures across the Taklamakan desert, Xinjiang (China), Iron Age burial mounds in Altai and Tianshan, Xinjiang (China), Thracian burial mounds and looted sites in Bulgaria, the Khanuy Valley and ice patches in Mongolia. Further research will also focus on the detectability of looting pits in high-resolution SAR imagery, through the development, setup, and running of an experiment based at the satellite receiving station of LIESMARS at Wuhan University, where looting structures will be created artificially to conduct tests of their detectability in HR and VHR SAR imagery.

Finally, new opportunities and perspectives brought by long-wavelength (e.g. BIOMASS P-band) and other VHR (e.g. IceEye and Paz X-band) SAR image products will also be explored, along with experiments aimed at further advancing image analysis approaches through the exploitation of Artificial Intelligence (AI), machine and deep learning techniques. These novel data and methods may offer unprecedented potential for heritage site monitoring in vegetated landscapes (using P-band data), for building-scale applications (using VHR imagery), and for semi-automated identification of assets and threats across wide regions (using AI and other advanced approaches).

Disclosure statement

No potential conflict of interest was reported by the author(s).

Funding

This work is supported by the European Space Agency (ESA) and the National Remote Sensing Center (NRSCC) – Ministry of Science and Technology (MOST) of the P.R. China under [grant number 58113], ESA [contract number 4000135360/21/I-NB, grant numbers 190791 and PP0085498], the German Aerospace Center (DLR) [grant number MTH3764], the Italian Space Agency (ASI) [COSMO-SkyMed license WUHAN-CSK], Planet Labs PBC under the Education and Research Program [grant number 412519], and the National Natural Science Foundation of China [grant number 42250610212].

Notes on contributors

Francesca Cigna is a senior researcher in Earth observation at the Institute of Atmospheric Sciences and Climate (ISAC), National Research Council (CNR) of Italy. She received the PhD degree in Earth Sciences from Florence University, Italy. Her research interests include SAR, advanced InSAR methods, data analytics, and monitoring of natural and anthropogenic hazards in urban and rural environments. She is the European Principal Investigator of the ESA-MOST Dragon-5 SARchaeology project.

Timo Balz is a professor for radar remote sensing at the State Key Laboratory of Information Engineering in Surveying, Mapping, and Remote Sensing (LIESMARS), Wuhan University, China. He received the PhD. degree in Aerospace Engineering and Geodesy from the University of Stuttgart, Germany. His research interests are SAR, mainly with respect to multi-baseline InSAR, as well as in using SAR for the support of archaeological prospection. He is the Chinese Principal Investigator of the ESA-MOST Dragon-5 SARchaeology project.

Deodato Tapete is a researcher in Earth observation and data analytics at the Italian Space Agency (ASI). He received the PhD degree in Earth Sciences from Florence University, Italy. His research interests include SAR data and InSAR techniques applied to natural hazards, urban remote sensing, archaeological prospection, and cultural heritage conservation. He is the European Co-Investigator of the ESA-MOST Dragon-5 SARchaeology project.

Gino Caspari is an honorary research associate at the Department of Archaeology, University of Sydney, Australia. He received the PhD degree in Archaeology from Hamburg University, Germany. His research interests include field archaeology, landscape archaeology, and archaeological remote sensing. He is a Chinese Co-Investigator of the ESA-MOST Dragon-5 SARchaeology project.

Bihong Fu is a research director at the Aerospace Information Research Institute (AIR), Chinese Academy of Sciences (CAS), China. He received the PhD degree in Earth Environment from Shizuoka University, China. His research interests include geomorphology, active tectonics, monitoring, and assessment of UNESCO heritage sites using optical remote sensing technologies. He is a Chinese Co-Investigator of the ESA-MOST Dragon-5 SARchaeology project.

Michele Abballe was a post-graduate research fellow at the Institute of Atmospheric Sciences and Climate (ISAC), National Research Council (CNR) of Italy, and a European Young Scientist of the ESA-MOST Dragon-5 SARchaeology project until March 2023. He is a PhD student in Arts and Archaeology at Ghent University, Belgium. His research interests include geoarchaeology, landscape archaeology, and GIS.

Haonan Jiang is a PhD student at Wuhan University in China and a visiting PhD student at the Helmholtz Centre Potsdam, GFZ German Research Centre for Geosciences, Germany. His research interests include using SAR remote sensing and InSAR to detect and analyze natural and anthropogenic hazards. He is a Chinese Young Scientist of the ESA-MOST Dragon-5 SARchaeology project.

ORCID

Francesca Cigna http://orcid.org/0000-0001-8134-1576
Timo Balz http://orcid.org/0000-0002-1624-4697
Deodato Tapete http://orcid.org/0000-0002-7242-4473
Gino Caspari http://orcid.org/0000-0002-0944-5095
Michele Abballe http://orcid.org/0000-0002-0557-1449
Haonan Jiang http://orcid.org/0000-0002-8036-4300

Data availability statement

The Earth Observation (EO) data that support the findings of this study are openly available from the European Space Agency (ESA) through Copernicus Open Access Hub (https://scihub.copernicus.eu/dhus), registration to the EO data access gateway, and via Third Party Mission announcements of opportunities (https://earth.esa.int/eogateway). OpenStreetMap® data are available under the Open Data Commons Open Database License (https://www.openstreetmap.org/copyright/en) by the OpenStreetMap Foundation (https://wiki.osmfoundation.org/wiki/Main_Page). Historical aerial photographs for the Province of Rome (Italy) are distributed by the National Archive of Aerial Photography – Central Institute for Cataloguing and Documentation (http://www.iccd.beniculturali.it/), or accessible via the Ministry of the Environment's national geoportal (http://www.pcn.minambiente.it/mattm/). Other datasets can be obtained through data license agreements with the Italian (ASI) and German (DLR) space agencies (https://www.asi.it/en/, https://www.dlr.de/en).

References

Agapiou, A., and V. Lysandrou. 2015. "Remote Sensing Archaeology: Tracking and Mapping Evolution in European Scientific Literature from 1999 to 2015." *Journal of Archaeological Science: Reports* 4:192–200. https://doi.org/10.1016/j.jasrep.2015.09.010.

Agapiou, A., V. Lysandrou, and D. G. Hadjimitsis. 2020. "Earth Observation Contribution to Cultural Heritage Disaster Risk Management: Case Study of Eastern Mediterranean Open Air Archaeological Monuments and Sites." *Remote Sensing* 12 (8): 1330. https://doi.org/10.3390/RS12081330.

Amenduni, G. 1884. "Sulle Opere Di Bonificazione Della Plaga Litoranea Dell'Agro Romano Che Comprende Le Paludi e Gli Stagni Di Ostia, Porto, Maccarese e Delle Terre Vallive Di Stracciacappa, Baccano, Pantano, Lago Dei Tartari." *Relazione Del Progetto Generale 15/7/1880*. Eredi Botta: Roma, Italy.

Bai, L., L. Jiang, H. Wang, and Q. Sun. 2016. "Spatiotemporal Characterization of Land Subsidence and Uplift (2009-2010) Over Wuhan in Central China Revealed by TerraSAR-X InSar Analysis." *Remote Sensing* 8 (4): 350. https://doi.org/10.3390/rs8040350.

Balz, T., G. Caspari, B. Fu, and M. Liao. 2016. "Discernibility of Burial Mounds in High-Resolution X-Band SAR Images for Archaeological Prospections in the Altai Mountains." *Remote Sensing* 8 (10): 817. https://doi.org/10.3390/rs8100817.

Benattou, M. M., T. Balz, and M. Liao. 2018. "Measuring Surface Subsidence in Wuhan, China with Sentinel-1 Data Using PSInSar." *International Archives of the Photogrammetry, Remote Sensing and Spatial Information Sciences - ISPRS Archives* 42 (3): 73–77. https://doi.org/10.5194/isprs-archives-XLII-3-73-2018.

Berardino, P., G. Fornaro, R. Lanari, and E. Sansosti. 2002. "A New Algorithm for Surface Deformation Monitoring Based on Small Baseline Differential SAR Interferograms." *IEEE Transactions on Geoscience and Remote Sensing* 40 (11): 2375–2383. https://doi.org/10.1109/TGRS.2002.803792.

Bini, M., I. Isola, G. Zanchetta, A. Ribolini, A. Ciampalini, I. Baneschi, D. Mele, and A. L. D'Agata. 2018. "Identification of Leveled Archaeological Mounds (Höyük) in the Alluvial Plain of the Ceyhan River (Southern Turkey) by Satellite Remote-Sensing Analyses." *Remote Sensing* 10 (2): 241. https://doi.org/10.3390/rs10020241.

Bozzano, F., C. Esposito, P. Mazzanti, M. Patti, and S. Scancella. 2018. "Imaging Multi-Age Construction Settlement Behaviour by Advanced SAR Interferometry." *Remote Sensing* 10 (7): 1137. https://doi.org/10.3390/rs10071137.

Campana, S. 2017. "Drones in Archaeology. State-Of-The-Art and Future Perspectives." *Archaeological Prospection* 24 (4): 275–296. https://doi.org/10.1002/arp.1569.

Campolunghi, M. P., G. Capelli, R. Funiciello, and M. Lanzini. 2007. "Geotechnical Studies for Foundation Settlement in Holocenic Alluvial Deposits in the City of Rome (Italy)." *Engineering Geology* 89 (1–2): 9–35. https://doi.org/10.1016/j.enggeo.2006.08.003 .

Caspari, G. 2018. "Assessing Looting from Space: The Destruction of Early Iron Age Burials in Northern Xinjiang." *Heritage* 1 (2): 320–327. https://doi.org/10.3390/heritage1020021.

Caspari, G., J. Blochin, T. Sadykov, and T. Balz. 2020. "Deciphering Circular Anthropogenic Anomalies in PALSAR Data-Using L-Band SAR for Analyzing Archaeological Features on the Steppe." *Remote Sensing* 12 (7): 1076. https://doi.org/10.3390/rs12071076 .

Caspari, G., T. Sadykov, J. Blochin, M. Bolliger, and S. Szidat. 2020. "New Evidence for a Bronze Age Date of Chariot Depictions in the Eurasian Steppe." *Rock Art Research* 37 (1): 53–58. https://doi.org/10.3316/ielapa.125642143820495.

Caspari, G., T. Sadykov, J. Blochin, M. Buess, M. Nieberle, and T. Balz. 2019. "Integrating Remote Sensing and Geophysics for Exploring Early Nomadic Funerary Architecture in the 'Siberian Valley of the Kings'." *Sensors (Switzerland)* 19 (14): 3074. https://doi.org/10.3390/s19143074.

Caspari, G., T. Sadykov, J. Blochin, and I. Hajdas. 2018. "Tunnug 1 (Arzhan 0) – an Early Scythian Kurgan in Tuva Republic, Russia." *Archaeological Research in Asia* 15:82–87. https://doi.org/10.1016/j.ara.2017.11.001.

Casu, F., S. Elefante, P. Imperatore, I. Zinno, M. Manunta, C. De Luca, and R. Lanari. 2014. "SBAS-DInsar Parallel Processing for Deformation Time-Series Computation." *IEEE Journal of Selected Topics in Applied Earth Observations and Remote Sensing* 7 (8): 3285–3296. https://doi.org/10.1109/JSTARS.2014.2322671.

Chan, A., T. Sadykov, J. Blochin, I. Hajdas, G. Caspari, and M. Novak. 2022. "The Polymorphism and Tradition of Funerary Practices of Medieval Turks in Light of New Findings from Tuva Republic." *PLOS ONE* 17 (9): e0274537. https://doi.org/10.1371/journal.pone.0274537.

Chen, F., H. Guo, D. Tapete, F. Cigna, S. Piro, R. Lasaponara, and N. Masini. 2022. "The Role of Imaging Radar in Cultural Heritage: From Technologies to Applications." *International Journal of Applied Earth Observation and Geoinformation* 112:102907. https://doi.org/10.1016/j.jag.2022.102907.

Chen, F., H. Guo, D. Tapete, N. Masini, F. Cigna, R. Lasaponara, S. Piro, H. Lin, and P. Ma. 2021. "Interdisciplinary Approaches Based on Imaging Radar Enable Cutting-Edge Cultural Heritage Applications." *National Science Review* 8 (9). Oxford University Press. https://doi.org/10.1093/nsr/nwab123.

Chen, F., H. Liu, H. Xu, W. Zhou, T. Balz, P. Chen, X. Zhu, H. Lin, C. Fang, and I. Parcharidis. 2021. "Deformation Monitoring and Thematic Mapping of the Badaling Great Wall Using Very High-Resolution Interferometric Synthetic Aperture Radar Data." *International Journal of Applied Earth Observation and Geoinformation* 105:102630. https://doi.org/10.1016/j.jag.2021.102630.

Chen, F., N. Masini, R. Yang, P. Milillo, D. Feng, and R. Lasaponara. 2015. "A Space View of Radar Archaeological Marks: First Applications of COSMO-Skymed X-Band Data." *Remote Sensing* 7 (1): 24–50./doi:10.3390/rs70100024. https://doi.org/10.3390/rs70100024.

Chen, F., W. Zhou, Y. Tang, R. Li, H. Lin, T. Balz, J. Luo, P. Shi, M. Zhu, and C. Fang. 2022. "Remote Sensing-Based Deformation Monitoring of Pagodas at the Bagan Cultural Heritage Site, Myanmar." *International Journal of Digital Earth* 15 (1): 770–788. https://doi.org/10.1080/17538947.2022.2062466.

Chen, L., X. Zhao, Y. Tang, and H. Zhang. 2018. "Parameters Fitting and Evaluation of Exponent Knothe Model Combined with InSar Technique." *Yantu Lixue/Rock and Soil Mechanics* 39 (S2): 423–431. https://doi.org/10.16285/j.rsm.2018.1426.

Chen, Z., S. Chen, and L. Wu. 2015. "Experimental Analysis of Soft Soil Characteristic in Wuhan." *Resources Environment and Engineering* 29 (6): 974–977.

Cigna, F., R. Lasaponara, N. Masini, P. Milillo, and D. Tapete. 2014. "Persistent Scatterer Interferometry Processing of COSMO-Skymed StripMap HIMAGE Time Series to Depict Deformation of the Historic Centre of Rome, Italy." *Remote Sensing* 6 (12): 12593–12618. https://doi.org/10.3390/rs61212593.

Cigna, F., and D. Tapete. 2018. "Tracking Human-Induced Landscape Disturbance at the Nasca Lines UNESCO World Heritage Site in Peru with COSMO-Skymed InSar." *Remote Sensing* 10 (4): 572. https://doi.org/10.3390/rs10040572.

Cigna, F., D. Tapete, R. Lasaponara, and N. Masini. 2013. "Amplitude Change Detection with ENVISAT ASAR to Image the Cultural Landscape of the Nasca Region, Peru." *Archaeological Prospection* 20 (2): 117–131. https://doi.org/10.1002/arp.1451 .

Conesa, F., A. Garcia-Molsosa, E. Angelats, and H. A. Orengo. 2022. "Cloud-Computing Procedures for the Automated Detection and Monitoring of Archaeological Sites." In *2022 IEEE Mediterranean and Middle-East Geoscience and Remote Sensing Symposium, M2GARSS 2022 - Proceedings*, 118–121. Institute of Electrical and Electronics Engineers Inc. https://doi.org/10.1109/M2GARSS52314.2022.9840013.

Costantini, M., J. Bai, F. Malvarosa, F. Minati, F. Vecchioli, R. Wang, Q. Hu, J. Xiao, and J. Li. 2016. "Ground Deformations and Building Stability Monitoring by COSMO-Skymed PSP SAR Interferometry: Results and Validation with Field Measurements and Surveys." In *International Geoscience and Remote Sensing Symposium (IGARSS)*, 6847–6850. https://doi.org/10.1109/IGARSS.2016.7730787.

Crosetto, M., O. Monserrat, M. Cuevas-González, N. Devanthéry, and B. Crippa. 2016. "Persistent Scatterer Interferometry: A Review." *ISPRS Journal of Photogrammetry and Remote Sensing* 115:78–89. https://doi.org/10.1016/j.isprsjprs.2015.10.011.

De Castro, F. R., A. Facciolo, M. Gala, M. C. Grossi, C. Morelli, M. L. Rinaldi, D. Ruggeri, and S. Sivilli. 2018. "La Sponda Destra Del Tevere, Presso La Foce, Prima Dei Romani: Gli Insediamenti." *La sponda destra del Tevere, presso la foce, prima dei Romani: gli insediamenti* 3–26. https://doi.org/10.4000/books.efr.3642.

Delgado Blasco, J. M., M. Foumelis, C. Stewart, and A. Hooper. 2019. "Measuring Urban Subsidence in the Rome Metropolitan Area (Italy) with Sentinel-1 SNAP-Stamps Persistent Scatterer Interferometry." *Remote Sensing* 11 (2): 129. https://doi.org/10.3390/rs11020129 .

Dong, X., Q. Xu, J. She, W. Li, F. Liu, and X. Zhou. 2020. "Preliminary Study on Interpretation of Geological Hazards in Jiuzhaigou Based on Multi-Source Remote Sensing Data." *Geomatics and Information Science of Wuhan University* 45 (3): 432–441. https://doi.org/10.13203/j.whugis20190076 .

Enei, F. 2001. *Progetto Ager Caeretanus: Il Litorale Di Alsium. Ricognizioni Archaeologiche Nel Territorio Di Ladispoli, Cerveteri e Fiumicino*.

Fan, Z., X. Gou, M. Qin, Q. Fan, J. Yu, and J. Zhao. 2018. "Information and Logistic Regression Models Based Coupling Analysis for Susceptibility of Geological Hazards." *Journal of Engineering Geology* 26 (2): 340–347. https://doi.org/10.13544/j.cnki.jeg.2017-052.

Ferretti, A., C. Colesanti, D. Perissin, C. Prati, and F. Rocca. 2004. "Evaluating the Effect of the Observation Time on the Distribution of SAR Permanent Scatterers." In *Proceedings of the FRINGE 2003 Workshop (ESA SP-550). 1-5 Dec 2003*, 167–172. Frascati, Italy: ESA/ESRIN. https://ui.adsabs.harvard.edu/abs/2004ESASP.550E.26F/abstract .

Ferretti, A., C. Prati, and F. Rocca. 2001. "Permanent Scatterers in SAR Interferometry." *IEEE Transactions on Geoscience and Remote Sensing* 39 (1): 8–20. https://doi.org/10.1109/36.898661.

Foumelis, M., T. Papadopoulou, P. Bally, F. Pacini, F. Provost, and J. Patruno. 2019. "Monitoring Geohazards Using On-Demand and Systematic Services on Esa's Geohazards Exploitation Platform." In *International Geoscience and Remote Sensing Symposium (IGARSS)*, 5457–5460. IEEE. https://doi.org/10.1109/IGARSS.2019.8898304.

Guo, J. Q., D. Peng, J. Cao, and J. Y. Yang. 2000. "Geomorphology and Quaternary Geology in Jiuzhai Valley." *Acta Geologica Sichuan* (3):183–192.

Guo, X., B. Fu, J. Du, P. Shi, Q. Chen, and W. Zhang. 2021. "Applicability of Susceptibility Model for Rock and Loess Earthquake Landslides in the Eastern Tibetan Plateau." *Remote Sensing* 13 (13): 2546. https://doi.org/10.3390/rs13132546.

Heinzelmann, M. 1998. "Beobachtungen Zur Suburbanen Topographie Ostias. Ein Orthogonales Straßensystem Im Bereich Der Pianabella." *Bullettino Dell'Istituto Archaeologico Germanico, Sezione Di Roma* 105. https://www.academia.edu/45437929/M_Heinzelmann_Beobachtungen_zur_suburbanen_Topographie_Ostias_Ein_orthogonales_Straßensystem_im_Bereich_der_Pianabella_RM_105_1998_175_225.

Jiang, H., T. Balz, F. Cigna, and D. Tapete. 2021. "Land Subsidence in Wuhan Revealed Using a Non-Linear PSInSar Approach with Long Time Series of COSMO-Skymed SAR Data." *Remote Sensing* 13 (7): 1256. https://doi.org/10.3390/rs13071256.

Jiang, H., T. Balz, F. Cigna, D. Tapete, J. Li, and Y. Han. 2023. "Multi-Sensor InSar Time Series Fusion for Long-Term Land Subsidence Monitoring." *Geo-Spatial Information Science* 1–17. https://doi.org/10.1080/10095020.2023.2178337.

Keay, S., M. Millett, L. Paroli, and K. D. Strutt. 2005. *Portus: An Archaeological Survey of the Port of Imperial Rome*. Rome, Italy: The British School at Rome.

Keay, S., M. Millett, K. Strutt, and P. Germoni. 2020. *The Isola Sacra Survey: Ostia, Portus and the Port System of Imperial Rome*. McDonald Institute for Archaeological Research. https://doi.org/10.17863/CAM.55280.

Keay, S., S. Parcak, and K. D. Strutt. 2014. "High Resolution Space and Ground-Based Remote Sensing and Implications for Landscape Archaeology: The Case from Portus, Italy." *Journal of Archaeological Science* 52:277–292. https://doi.org/10.1016/j.jas.2014.08.010.

Keay, S., and L. Paroli. 2011. *Portus and Its Hinterland: Recent Archaeological Research*. London: British School at Rome.

Lanari, R., O. Mora, M. Manunta, J. J. Mallorquí, P. Berardino, and E. Sansosti. 2004. "A Small-Baseline Approach for Investigating Deformations on Full-Resolution Differential SAR Interferograms." *IEEE Transactions on Geoscience and Remote Sensing* 42 (7): 1377–1386. https://doi.org/10.1109/TGRS.2004.828196.

Lasaponara, R., N. Abate, and N. Masini. 2022. "On the Use of Google Earth Engine and Sentinel Data to Detect "Lost" Sections of Ancient Roads. The Case of via Appia." *IEEE Geoscience and Remote Sensing Letters* 19:1–5. https://doi.org/10.1109/LGRS.2021.3054168.

Lasaponara, R., and N. Masini. 2012. "Satellite Remote Sensing: A New Tool for Archaeology." In *Remote Sensing and Digital Image Processing*, edited by R. Lasaponara and N. Masini, 16. Netherlands: Springer. https://doi.org/10.1007/978-90-481-8801-7.

Luo, L., X. Wang, H. Guo, R. Lasaponara, P. Shi, N. Bachagha, L. Li, et al. 2018. "Google Earth as a Powerful Tool for Archaeological and Cultural Heritage Applications: A Review." *Remote Sensing* 10 (10): 1558. https://doi.org/10.3390/rs10101558.

Luo, L., X. Wang, H. Guo, R. Lasaponara, X. Zong, N. Masini, G. Wang, et al. 2019. "Airborne and Spaceborne Remote Sensing for Archaeological and Cultural Heritage

Applications: A Review of the Century (1907–2017)." *Remote Sensing of Environment* 232:111280. https://doi.org/10.1016/j.rse.2019.111280.

Luo, X. J. 2014. "Division of 'Six Belts and Five Types' of Carbonate Region and Control of Karst Geological Disaster in Wuhan." *Journal of Hydraulic Engineering* 45 (2): 171–179. https://doi.org/10.13243/j.cnki.slxb.2014.02.006.

Manunta, M., C. De Luca, I. Zinno, F. Casu, M. Manzo, M. Bonano, A. Fusco, et al. 2019. "The Parallel SBAS Approach for Sentinel-1 Interferometric Wide Swath Deformation Time-Series Generation: Algorithm Description and Products Quality Assessment." *IEEE Transactions on Geoscience & Remote Sensing* 57 (9): 6259–6281. https://doi.org/10.1109/TGRS.2019.2904912.

McGrath, C. N., C. Scott, D. Cowley, and M. Macdonald. 2020. "Towards a Satellite System for Archaeology? Simulation of an Optical Satellite Mission with Ideal Spatial and Temporal Resolution, Illustrated by a Case Study in Scotland." *Remote Sensing* 12 (24): 1–19. https://doi.org/10.3390/rs12244100.

Miano, A., F. Di Carlo, A. Mele, I. Giannetti, N. Nappo, M. Rompato, P. Striano, et al. 2022. "GIS Integration of DInSAR Measurements, Geological Investigation and Historical Surveys for the Structural Monitoring of Buildings and Infrastructures: An Application to the Valco San Paolo Urban Area of Rome." *Infrastructures* 7 (7): 89. https://doi.org/10.3390/infrastructures7070089.

Milella, M., G. Caspari, Y. Kapinus, T. Sadykov, J. Blochin, A. Malyutina, M. Keller, et al. 2021. "Troubles in Tuva: Patterns of Perimortem Trauma in a Nomadic Community from Southern Siberia (Second to Fourth C. CE)." *American Journal of Physical Anthropology* 174 (1): 3–19. https://doi.org/10.1002/ajpa.24142 .

Morelli, C. 2014. "L'Ager Portuensis. La Dimensione Territoriale Dei Contesti Archaeologici." In *Paesaggi Dell'archaeologia Invisibile. Il Caso Del Distretto Portuense*, edited by L. Caravaggi and C. Morelli, 52–68. Recanati, Italy: Quodlibet.

Morelli, C. 2020. "The Campus Salinarum Romanarum." In *Life and Death in a Multicultural Harbour City: Ostia Antica from the Republic Through Late Antiquity. Acta Instituti Romani Finlandiae 47. Quasar, Roma*, edited by A. Karivieri, 231–242. Rome, Italy: British School at Rome.

Morelli, C., A. Carbonara, V. Forte, M. C. Grossi, and A. Arnoldus-Huyzendveld. 2011. "La Topografia Romana Dell'Agro Portuense Alla Luce Delle Nuove Indagini." In *Portus and Its Hinterland: Recent Archaeological Research*, edited by S. Keay and L. Paroli, 261–285. Archaeological Monographs of the British School at Rome. London: British School at Rome in collaboration with the Soprintendenza speciale per i beni archaeologici di Roma, sede di Ostia. http://www.ostia-antica.org/fulltext/morelli/morelli-2011.pdf.

Orengo, H. A., F. C. Conesa, A. Garcia-Molsosa, A. Lobo, A. S. Green, M. Madella, and C. A. Petrie. 2020. "Automated Detection of Archaeological Mounds Using Machine-Learning Classification of Multisensor and Multitemporal Satellite Data." *Proceedings of the National Academy of Sciences of the United States of America* 117 (31): 18240–18250. https://doi.org/10.1073/pnas.2005583117 .

Qu, X., J. Yang, and M. Chang. 2019. "A Deep Learning Model for Concrete Dam Deformation Prediction Based on RS-LSTM." *Journal of Sensors* 2019:1–14. https://doi.org/10.1155/2019/4581672 .

Raspini, F., S. Bianchini, S. Moretti, C. Loupasakis, D. Rozos, J. Duro, and M. Garcia. 2016. "Advanced Interpretation of Interferometric SAR Data to Detect, Monitor and Model Ground Subsidence: Outcomes from the ESA-GMES Terrafirma Project." *Natural Hazards* 83 (1): 155–181. https://doi.org/10.1007/s11069-016-2341-x.

Rayne, L., M. C. Gatto, L. Abdulaati, M. Al-Haddad, M. Sterry, N. Sheldrick, and D. Mattingly. 2020. "Detecting Change at Archaeological Sites in North Africa Using Open-Source Satellite Imagery." *Remote Sensing* 12 (22): 1–29. https://doi.org/10.3390/rs12223694 .

Ruescas, A. B., J. M. Delgado Blasco, F. Costantini, and F. Sarti. 2009. "Change Detection by Interferometric Coherence in Nasca Lines, Peru (1997–2004)." In *Proceedings of the Fringe 2009 Workshop*, Frascati, Italy, 30 November 2009–4 December 2009, 7.

Sadykov, T., G. Caspari, and J. Blochin. 2020. "Kurgan Tunnug 1—New Data on the Earliest Horizon of Scythian Material Culture." *Journal of Field Archaeology* 45 (8): 556–570. https://doi.org/10.1080/00934690.2020.1821152.

Sadykov, T., G. Caspari, J. Blochin, S. Lösch, Y. Kapinus, M. Milella, and P. F. Biehl. 2021. "The Kokel of Southern Siberia: New Data on a Post-Xiongnu Material Culture." *PLoS ONE* 16 (7): e0254545. https://doi.org/10.1371/journal.pone.0254545.

Stramondo, S., F. Bozzano, F. Marra, U. Wegmuller, F. R. Cinti, M. Moro, and M. Saroli. 2008. "Subsidence Induced by Urbanisation in the City of Rome Detected by Advanced InSAR Technique and Geotechnical Investigations." *Remote Sensing of Environment* 112 (6): 3160–3172. https://doi.org/10.1016/j.rse.2008.03.008.

Talledo, D. A., A. Miano, M. Bonano, F. Di Carlo, R. Lanari, M. Manunta, A. Meda, et al. 2022. "Satellite Radar Interferometry: Potential and Limitations for Structural Assessment and Monitoring." *Journal of Building Engineering* 46:103756. https://doi.org/10.1016/j.jobe.2021.103756.

Tapete, D., and F. Cigna. 2017a. "InSAR Data for Geohazard Assessment in UNESCO World Heritage Sites: State-Of-The-Art and Perspectives in the Copernicus Era." *International Journal of Applied Earth Observation and Geoinformation* 63:24–32. https://doi.org/10.1016/j.jag.2017.07.007.

Tapete, D., and F. Cigna. 2017b. "Trends and Perspectives of Space-Borne SAR Remote Sensing for Archaeological Landscape and Cultural Heritage Applications." *Journal of Archaeological Science: Reports* 14:716–726. https://doi.org/10.1016/j.jasrep.2016.07.017.

Tapete, D., and F. Cigna. 2018. "Appraisal of Opportunities and Perspectives for the Systematic Condition Assessment of Heritage Sites with Copernicus Sentinel-2 High-Resolution Multispectral Imagery." *Remote Sensing* 10 (4): 561. https://doi.org/10.3390/rs10040561.

Tapete, D., and F. Cigna. 2019a. "COSMO-Skymed SAR for Detection and Monitoring of Archaeological and Cultural Heritage Sites." *Remote Sensing* 11 (11): 1326. https://doi.org/10.3390/rs11111326.

Tapete, D., and F. Cigna. 2019b. "Detection of Archaeological Looting from Space: Methods, Achievements and Challenges." *Remote Sensing* 11 (20): 2389. https://doi.org/10.3390/rs11202389.

Tapete, D., and F. Cigna. 2020. "Poorly Known 2018 Floods in Bosra UNESCO Site and Sergiopolis in Syria Unveiled from Space Using Sentinel-1/2 and COSMO-Skymed."

Scientific Reports 10 (1): 1–16. https://doi.org/10.1038/s41598-020-69181-x .

Tapete, D., F. Cigna, T. Balz, H. Tanveer, J. Wang, and H. Jiang. 2021a. "Multi-Temporal InSAR and Target Detection with COSMO-Skymed SAR Big Data to Monitor Urban Dynamics in Wuhan (China)." In *International Geoscience and Remote Sensing Symposium (IGARSS)*, 3793–3796. Institute of Electrical and Electronics Engineers Inc. https://doi.org/10.1109/IGARSS47720.2021.9554360 .

Tapete, D., F. Cigna, and D. N. M. Donoghue. 2016. "'Looting Marks' in Space-Borne SAR Imagery: Measuring Rates of Archaeological Looting in Apamea (Syria) with TerraSAR-X Staring Spotlight." *Remote Sensing of Environment* 178:42–58. https://doi.org/10.1016/j.rse.2016.02.055.

Tapete, D., F. Cigna, N. Masini, and R. Lasaponara. 2013. "Prospection and Monitoring of the Archaeological Heritage of Nasca, Peru, with ENVISAT ASAR." *Archaeological Prospection* 20 (2): 133–147. https://doi.org/10.1002/arp.1449 .

Tapete, D., R. Fanti, R. Cecchi, P. Petrangeli, and N. Casagli. 2012. "Satellite Radar Interferometry for Monitoring and Early-Stage Warning of Structural Instability in Archaeological Sites." *Journal of Geophysics and Engineering* 9 (4): S10–25. https://doi.org/10.1088/1742-2132/9/4/S10 .

Tapete, D., S. Morelli, R. Fanti, and N. Casagli. 2015. "Localising Deformation Along the Elevation of Linear Structures: An Experiment with Space-Borne InSAR and RTK GPS on the Roman Aqueducts in Rome, Italy." *Applied Geography* 58:65–83. https://doi.org/10.1016/j.apgeog.2015.01.009.

Tapete, D., A. Traviglia, E. Delpozzo, and F. Cigna. 2021b. "Regional-Scale Systematic Mapping of Archaeological Mounds and Detection of Looting Using COSMO-Skymed High Resolution DEM and Satellite Imagery." *Remote Sensing* 13 (16): 3106. https://doi.org/10.3390/rs13163106.

Wilson, D. R. 2000. *Air Photo Interpretation for Archaeologists*. Tempus Publishing Ltd.

Wiseman, J., and F. El-Baz. 2007. *Remote Sensing in Archaeology*. New York: Springer. https://doi.org/10.1007/0-387-44455-6.

Wu, C., P. Cui, Y. Li, I. A. Ayala, C. Huang, and S. Yi. 2018. "Seismogenic Fault and Topography Control on the Spatial Patterns of Landslides Triggered by the 2017 Jiuzhaigou Earthquake." *Journal of Mountain Science* 15 (4): 793–807. https://doi.org/10.1007/s11629-017-4761-9.

Wu, H., W. C. Cheng, S. L. Shen, M. Y. Lin, and A. Arulrajah. 2020. "Variation of Hydro-Environment During Past Four Decades with Underground Sponge City Planning to Control Flash Floods in Wuhan, China: An Overview." *Underground Space (China)* 5 (2): 184–198. https://doi.org/10.1016/j.undsp.2019.01.003.

Zanni, S., and A. De Rosa. 2019. "Remote Sensing Analyses on Sentinel-2 Images: Looking for Roman Roads in Srem Region (Serbia)." *Geosciences (Switzerland)* 9 (1): 25. https://doi.org/10.3390/geosciences9010025.

Zevi, F. 1996. "Sulle Fasi Più Antiche Di Ostia." In *"Roman Ostia" Revisited. Archaeological and Historical Papers in Memory of Russell Meiggs*, edited by A. Gallina, F. Zevi, and A. Claridge, 69–89. Rome, Italy: British School at Rome.

Zhou, L., J. Guo, J. Hu, J. Li, Y. Xu, Y. Pan, and M. Shi. 2017. "Wuhan Surface Subsidence Analysis in 2015–2016 Based on Sentinel-1A Data by SBAS-InSAR." *Remote Sensing* 9 (10): 982. https://doi.org/10.3390/rs9100982.